

http://pubs.acs.org/journal/aelccp

# Processing Strategies to Improve Cell-Level Energy Density of Metal Sulfide Electrolyte-Based All-Solid-State Li Metal Batteries and Beyond

Daxian Cao, Yuyue Zhao, Xiao Sun, Avi Natan, Ying Wang, Pengyang Xiang, Wei Wang, and Hongli Zhu\*



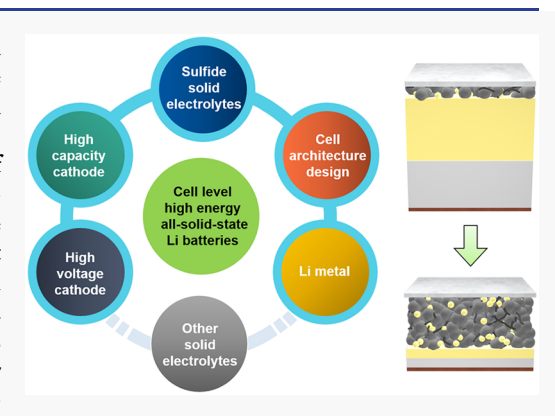
Cite This: ACS Energy Lett. 2020, 5, 3468-3489



**ACCESS** I

III Metrics & More

ABSTRACT: All-solid-state Li metal batteries (ASLBs) have the potential to surpass the energy density of commercial Li ion batteries and improve safety. However, most reported ASLBs deliver unsatisfactory cell-level energy densities, which are significantly affected by cell configuration. Therefore, for the first time, this Review summarized the processing of ASLBs toward cell-level high energy, with a focus on using sulfide solid-state electrolytes (SEs). We comprehensively analyzed the effects of the cathode, electrolyte, and Li metal anode on the energy density. Different strategies for the fabrication of thick cathode, thin electrolyte, and thin Li metal were systematically introduced, and their corresponding merits and challenges were summarized. In addition, the architectural design of ASLBs was discussed. Furthermore, we covered the most recent developments for other promising electrolytes. Finally, perspectives on the design of high-energy ASLBs toward practical applications were introduced.



Article Recommendations

To meet the increasing demand for electric vehicles and portable electronics, there has been a greater focus on developing higher energy density and safer energy storage devices. Greater energy density is favorable to provide longer usage time after one charge, space-savings, and low weight. Compared with other conventional batteries, like leadacid, nickel-metal hydride, and flow batteries, Li ion batteries (LIBs) play a critical role in modern society, because of their high energy (100-265 Wh kg<sup>-1</sup> or 250-670 Wh L<sup>-1</sup>), long cycle life (>1000 cycles), and low cost (<250 US\$ kWh<sup>-1</sup>).<sup>1,2</sup> However, state-of-the-art LIBs, which have transition metal oxide cathodes, graphite anodes, and organic liquid electrolyte (OLEs), have reached their upper limit of energy density. Whereas, combustion engines in automobiles which use gasoline deliver a high energy density (>1000 Wh kg<sup>-1</sup>).<sup>3</sup> The U.S. Department of Energy and U.S. Advanced Battery Consortium has set a goal for cell-level batteries used in electric vehicles at 350 Wh kg<sup>-1</sup> and 750 Wh L<sup>-1</sup>. Meanwhile, the frequently reported issues caused by OLEs, such as thermal runaway and explosion, lead to concerns about LIB safety risks. 5,6 Therefore, it is urgent to develop high-energy and safe batteries for the next generation of energy storage.

All-solid-state Li metal batteries (ASLBs) that couple solidstate electrolytes (SEs) with Li metal anode are promising for new strategies exhibiting nonflammability and promising energy density. While the traditional graphite anode has a limited capacity (378 mAh g<sup>-1</sup>), Li metal anode has gained interest from academia to industry because of its ultrahigh capacity (3860 mAh g<sup>-1</sup>) and low reduction potential (-3.04 V vs standard hydrogen electrode).<sup>7</sup> However, when used in OLEs, the Li metal anode has an uneven deposition, which leads to the growth of dendrites that may easily penetrate the separator and cause an internal short circuit of the battery.<sup>8</sup> Therefore, SEs owning high modulus are sought to suppress dendritic growth and achieve better utilization of Li metal.<sup>9</sup> Moreover, SEs can promote some low-cost and high-capacity

Received: September 3, 2020 Accepted: October 2, 2020 Published: October 19, 2020





© 2020 American Chemical Society

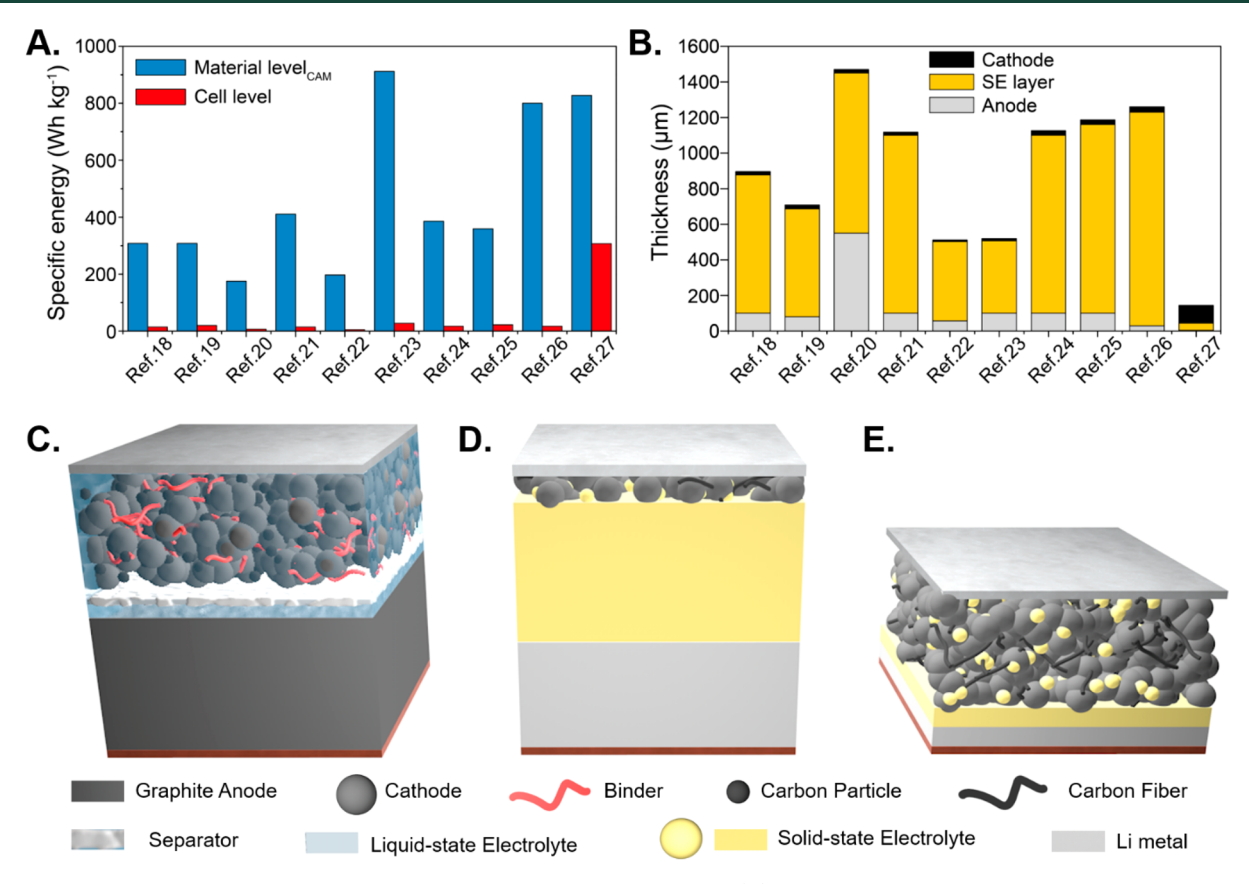


Figure 1. Relationship between cell configuration and cell-level energy in ASLBs. (A) Comparison in specific energy between active material level and cell level. (B) Thicknesses of each layer in reported ASLBs. <sup>29</sup> Data of Ref. 18–25 come from ref 29. Reproduced with permission from ref 29. Copyright 2020 Springer Nature. Data of ref. 26 and ref. 27 are combined and plotted. Typical configurations of (C) conventional LIBs, (D) current ASLBs, and (E) future high-energy ASLBs.

cathodes, such as sulfur (1675 mAh g<sup>-1</sup>) and metal sulfide like FeS<sub>2</sub> (894 mAh g<sup>-1</sup>), because the natural solid state can intrinsically address the shuttle effect and mitigate the mass loss of active material in OLEs. 10,111 The match of Li and sulfur could generate the theoretical specific energy as high as 2567 Wh kg<sup>-1</sup>, which is remarkably higher than that of conventional graphite-LiCoO2 batteries (theoretical specific energy density of 387 Wh kg<sup>-1</sup>). 12

Among various candidates, sulfide SEs are one of the most promising SEs to realize the operation of ASLBs at RT without sacrificing performance because of comparable IC with OLEs (>10<sup>-3</sup> S cm<sup>-1</sup>) and high processability. 13-15 However, there are challenges when sulfide SE is applied to ASLBs, especially when paring with Li metal anode and high-voltage cathode. For example, some sulfide SEs, like Li<sub>10</sub>GeP<sub>2</sub>S<sub>12</sub> and  $\text{Li}_{9.54}\text{Si}_{1.74}\text{P}_{1.44}\text{S}_{11.7}\text{Cl}_{0.3}$ , have exceedingly high IC >  $10^{-2}$  S cm<sup>-1</sup> but suffer from narrow electrochemical stability windows (ESWs) (1.7-2.3 V (vs Li<sup>+</sup>/Li)), chemical reactions with transition metal oxide cathodes and Li metal anodes, and the formation of a space charge layer against electrodes. 16 More importantly, recent work has proved that Li metal is still able to propagate sulfide SE and leads to a short circuit at a low critical current density (CCD), which is even more severe than in OLEs.<sup>17</sup> Tremendous efforts have been made to investigate the failure mechanisms, and some strategies, like interface engineering, element-doping of SEs, and compositing with polymers, can effectively address the aforementioned challenges or remit them to some extent.5,7 Using these strategies, outstanding energy density (>900 Wh kg<sup>-1</sup>) based on active

materials is achieved, as shown in Figure 1A. 18-27 However, the energy density in most reported ASLBs is much lower than expected after consideration at cell level (<50 Wh kg<sup>-1</sup>), which is much lower than that of commercial LIBs ( $\sim$ 250 Wh kg<sup>-1</sup>). As rapid progress has been made on ASLBs, it is significant to reduce the difference between the energy density from the material level to the cell level.

The calculation of energy density in cell level includes the mass of cathode active material (CAM), anode active material (AAM), electrolyte, additives (binder and conductive additives), current collectors, and even pack. Figure 1B displays the layer thickness of each component in some representative work. Generally, in the lab scale, the SE layer has a thickness of  $\sim 500 \, \mu \text{m}$ , an area less than 1.5 cm<sup>2</sup>, and a weight of approximately 200 mg, whereas the CAM weighs less than 20 mg. Therefore, the specific energy dramatically reduces because of the enormous weight difference between the material and cell level from the thick and heavy SE layer. This also explains the massive drop in energy density when transferring from conventional LIBs (Figure 1C) to current ASLBs (Figure 1D). Moreover, the mass loading of CAM significantly affects the areal energy density, a significant indicator of the cell size of ASLB. Unfortunately, a low mass loading of CAM is applied in most reported ASLBs to promote charge accessibility and achieve an optimized specific capacity. Furthermore, considering flooded Li is often employed in ASLBs, which will further reduce the energy density in the cell level; thus, reducing the thickness of Li metal to an acceptable level could effectively boost the volumetric energy density.

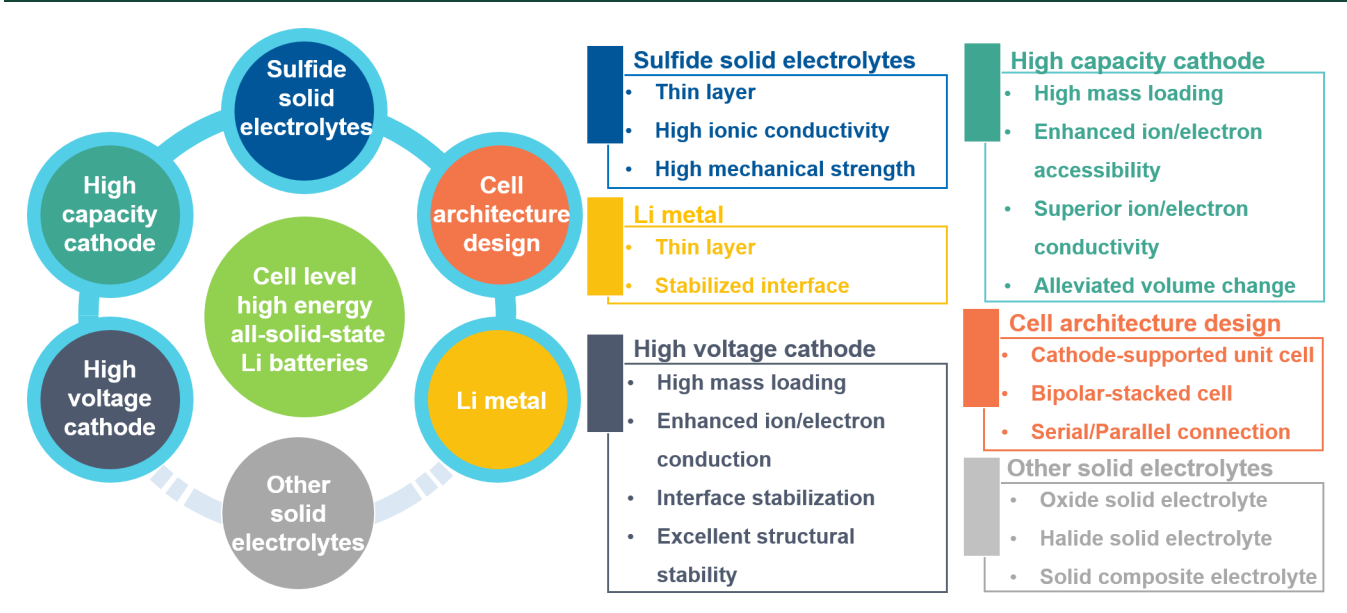


Figure 2. Scope of this Review. Components, including sulfide solid electrolyte, high-voltage cathode, high-capacity cathode, Li metal, cell architecture design, and other solid electrolytes, are specially designed to achieve cell-level high-energy all-solid-state Li metal batteries.

Other challenges for the Li metal anode utilization are their stability with sulfide SEs and issues with dendrite formation. Interface stabilization and dendrite suppression are prerequisites for the employment of a thin Li metal anode. Therefore, developing a thin SE; thick cathode; and thin, stabilized Li metal anode is essential to enable cell-level high-energy ASLBs, as illustrated in Figure 1E.

Very recently, Randau et al. quantitatively evaluated the energy density from material level to cell level and reported benchmarks for several key parameters in developing highenergy ASLBs, such as thin electrolyte layer ( $<30 \mu m$ ), low internal areal resistance ( $<40 \Omega \text{ cm}^2$ ), high areal capacity (>5mAh cm<sup>-2</sup>), and theoretical cathode specific energy (>500 Wh kg<sup>-1</sup>).<sup>29</sup> Meanwhile, Lee et al. reported a pioneering work that utilized a thick cathode layer (100  $\mu$ m), an ultrathin electrolyte layer (30  $\mu$ m), and an anode-free design.<sup>27</sup> A notable performance (>900 Wh l<sup>-1</sup>, >1000 cycles) was achieved in the Ah class pouch cell. Herein, instead of focusing on the more commonly covered challenges related to materials chemistry, this Review will uniquely discuss solutions to improve the cell-level energy density of ASLBs through processing. In the following sections, we will systematically analyze the effect of cathode configurations, electrolyte interlayer, and Li metal anode on the energy density. Different strategies specifically focused on the fabrication of thick cathode electrode, ultrathin electrolyte interlayer, and stabilized lithium metal anode with small thickness will be introduced. The corresponding merits and challenges will be summarized. In addition, the architecture design of ASLBs will be discussed. Meanwhile, the progress of other promising electrolytes will be briefly introduced. In the end, we present perspectives regarding the design of sulfide electrolyte-based ASLBs and some challenges faced in the development toward practical application. The scope of this Review is presented in Figure 2.

1. Electrolyte Design for High-Energy Sulfide Electrolyte-Based ASLBs. To optimize cell-level energy density of ASLBs, one of the keys is to construct a thin and stable electrolyte layer. Compared with other ceramic SEs, like oxides and phosphates, sulfide SEs have outstanding processability

because of their relatively softer nature. However, the natural sensitivity to moisture and many common organic solvents limits the number of promising process approaches. The most adopted fabrication approach is cold pressing, which often builds a pallet with a thickness greater than 500  $\mu$ m. When reducing thickness, the major challenge is the brittleness of the ceramic electrolyte layer, especially in the case of low thickness to area ratios (such as 0.001, assuming the thickness, length, and width are 50  $\mu$ m  $\times$  10 cm  $\times$  5 cm). Therefore, inspired by the binder-assisted electrode fabrication in conventional LIBs, combining polymeric binders or templates with sulfide SEs is a promising strategy to prepare thin sulfide SE layers with good mechanical strength. The introduction of binders or templates can also enhance the SE's mechanical strength, especially in large-scale roll-to-roll manufacturing processes. In this part, several promising approaches for SE layer fabrication are introduced and their corresponding advantages and disadvantages are discussed in detail.

1.1. Thin Solid Electrolyte Layer Prepared with Binders through Slurry Coating Method. Slurry coating is a conventional method for LIB electrode fabrication. As illustrated in Figure 3A(a), the slurry made of target particles and binders in a solvent was cast on the current collectors through the doctor blade, and a robust layer with uniform thickness was prepared after evaporation of the solvent and subsequent pressing. However, several limitations hinder the fabrication of sulfide SE layers by using the slurry method. Sulfide SEs are highly sensitive to conventional solvents, like water, N-methyl-2-pyrrolidone (NMP), acetonitrile (ACN), tetrahydrofuran (THF), N,Ndimethylformamide (DMF), etc.<sup>30</sup> When exposed to water, sulfide SEs rapidly decompose accompanied by the generation of toxic H<sub>2</sub>S gas.<sup>31</sup> The interaction with those mentioned organic polar solvents dramatically degrade the IC of SEs. A high-temperature annealing processing (>200 °C) is necessary to recover the IC, which is challenging for most polymeric binders and templates which typically have low melting points. Therefore, nonpolar or less polar solvents, such as toluene, xylene, pentane, and hexane, are employed to prepare stable sulfide SE slurries. However, highly effective binders, such as polyvinylidene fluoride (PVDF), carboxymethyl cellulose

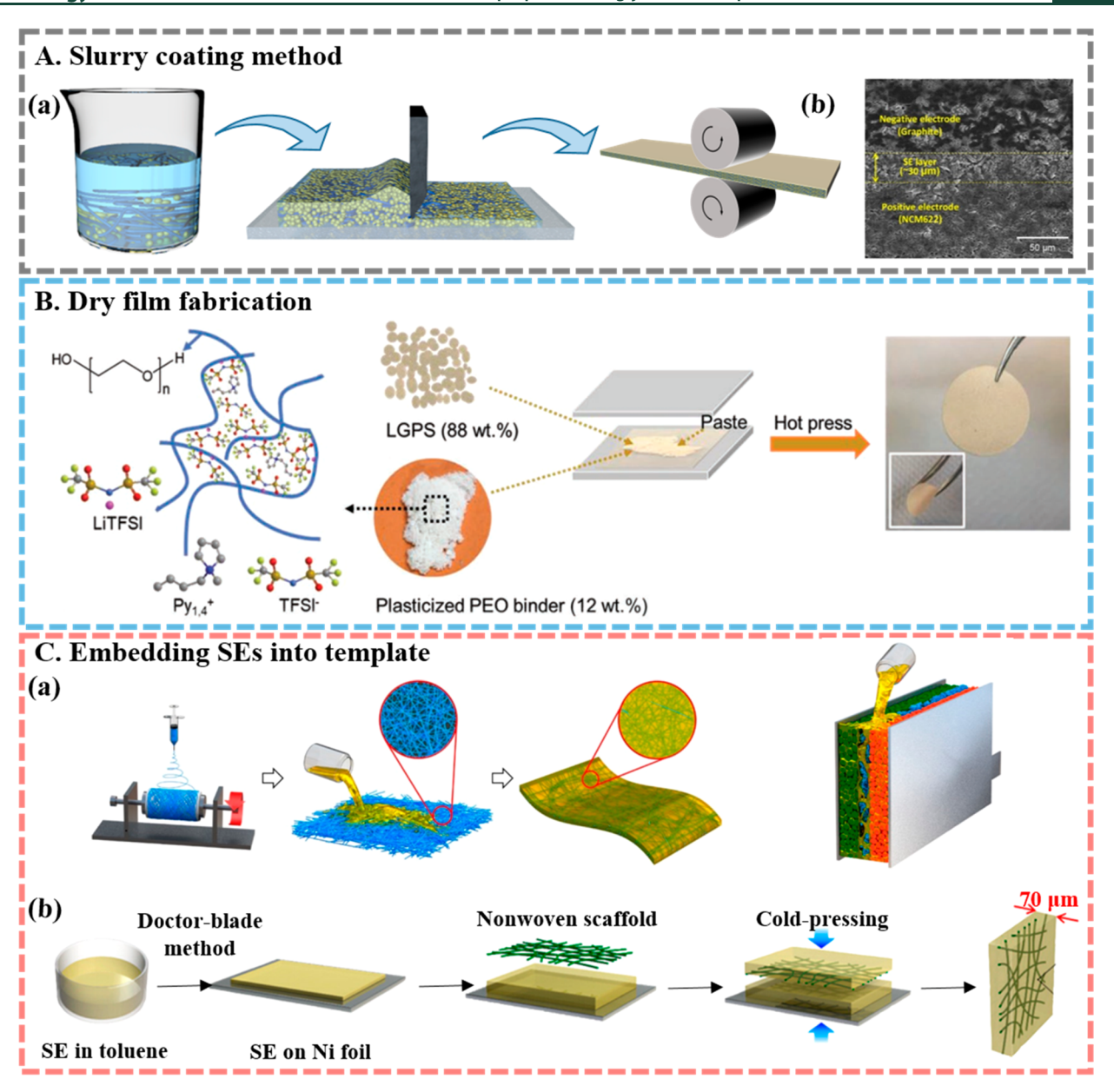


Figure 3. Fabrication of thin SE layer with (A) slurry coating method. (a) Schematic illustration of the process including slurry preparation, coating, and pressing. (b) SEM image to show the thin SE layer.<sup>33</sup> (Reproduced with permission from ref 33. Copyright 2018 Elsevier B.V.) (B) Dry film fabrication.<sup>34</sup> (Reproduced with permission from ref 34. Copyright 2020 Wiley VCH.) (C) Embedding SEs into templates via (a) infiltration of SE solution into electrospun membrane<sup>37</sup> (Reproduced with permission from ref 37. Copyright 2020 American Chemical Society.) and (b) pressing dry SE film with a scaffold.<sup>38</sup> (Reproduced with permission from ref 38. Copyright 2015 American Chemical Society.)

(CMC), and poly(vinyl alcohol) (PVA), must be dissolved in polar solvents, such as NMP and water, because these polymers have limited solubility in nonpolar solvents. Therefore, it is challenging to find binders that balance solubility and effective binding ability. In addition, the IC of the SE layer will decrease to some extent because of the introduction of binders. Most polymeric binders without IC hinder ion conduction in the SE layer, which leads to higher impedance in the ASLBs. Therefore, the selection of solvents and binders is critical for the slurry-processed sulfide SE layer.

Rubbers have garnered significant interest as an SE binder because of their good solubility in nonpolar xylene and considerable binding effect. As early as 2003, Inada et al. reported the employment of styrene—butadiene rubber (SBR)

and silicon rubber (SR) as binders and xylene as the solvent to fabricate sulfide SEs layers. In their work, the SE layer exhibited decreased IC after adding binders, which was attributed to the SBR probably wrapping the SE particles and blocking ion conduction. Recently, Nam et al. reported SE layers with a thickness of 30  $\mu$ m using nitrile butadiene rubber (NBR) as the binder and xylene as the solvent, as shown in Figure 3A(b). Because of the binder's negative effect on ion conductivity, the specific capacity decreased by 18–35 mAh g<sup>-1</sup> compared with the one without the binder. Very recently, Lee et al. reported a new system that employs nonaqueous acrylate-type binder and a mixture solvent of xylene and isobutyl isobutyrate. After pressurization through warm isostatic pressing (WIP) and optimization in the solvent, a

flexible SE film with a thickness of 30  $\mu$ m was achieved and delivered considerable mechanical strength and pinhole-free quality. More impressively, the IC decreased only slightly from  $1.8 \times 10^{-3}$  to  $1.31 \times 10^{-3}$  S cm<sup>-1</sup> at RT, comparable with the value of SE sheets fabricated through cold pressing.

1.2. Thin Solid Electrolyte Layer Prepared by Dry Processing Method. To eliminate the limitation of solvents when adding binders, a dry processing method is suggested. As illustrated in Figure 3B, Li et al. developed a plasticized PEO binder to enable the thin electrolyte fabrication based on  $\text{Li}_{3.25}\text{Ge}_{0.25}\text{P}_{0.75}\text{S}_4$  (LGPS). The PEO electrolyte is more amorphous after plasticization by  $\text{Py}_{1.4}\text{TFSI}$ , which increases the binding effect when composited with LGPS. As a result, after hot pressing, a free-standing layer was achieved with a thickness of around 100  $\mu\text{m}$ . Though the IC decreased a little from 2.81 to 0.42 mS cm<sup>-1</sup>, it showed good interfacial wetting and stability with Li metal during cycling.

Moreover, in comparison with using sticky binders to improve the film formability, introducing fabric or mesh to the sulfide SEs is another strategy to enhance the mechanical strength of the thin SE layer. Yersak et al. introduced aramid fibers into  $(\text{Li}_2\text{S})_{70}(\text{P}_2\text{S}_5)_{30}$ , and a thin electrolyte with a thickness of 100  $\mu\text{m}$  was achieved. The hot pressing at 240 °C and 200 MPa is vital in the fabrication because the softened sulfide glass could flow around the rigid aramid fibers to achieve intimate contact. The resultant film is further densified. Impressively, the layer with 10 wt % aramid fiber was mechanically robust and delivered a high IC of 2.4 mS cm<sup>-1</sup>.

1.3. Embedding Sulfide Electrolyte into Templates as Thin Solid Electrolyte Layer. Embedding sulfide SEs into a template owning interconnected pores is another promising approach to reduce electrolyte thickness, which is based on the unique properties of sulfide SEs, as illustrated in Figure 3C. Some sulfide SEs are synthesized through the wet chemical method, while some of them can be directly dissolved in certain solvents. 30,36 This solution-based method enables SEs to infiltrate the template.<sup>32</sup> Meanwhile, the relatively soft property of sulfide SEs allows it to be pressed into a robust template. In this configuration, the ion conductivity is attributed to sulfide SEs, whereas the template provides mechanical strength. Some properties of the template, such as the tortuosity of inside pores, thermal stability, chemical stability, mechanical strength, and so on, are critical to the performance of the SE layer. In this section, template utilization methods will be discussed from wet solution infiltration to dry mechanical pressing.Developing thin, robust, and highly ion conductive electrolyte layers is the key to achieving cell-level high energy density.

Developing thin, robust, and highly ion conductive electrolyte layers is the key to achieving cell-level high energy density.

As aforementioned, some sulfide SEs are synthesized through a solution method followed by low-temperature annealing (<300 °C). The annealing treatment is important to remove the remaining solvent completely. Therefore, one of the critical parameters for the template is good thermal stability. Recently, Kim et al. fabricated a thin electrolyte (40–70  $\mu$ m in thickness) through the infiltration of solution-based Li<sub>6</sub>PS<sub>5</sub>Cl<sub>0.5</sub>Br<sub>0.5</sub> into electrospun polyimide nonwovens (NW),

as illustrated in Figure 3C(a).<sup>37</sup> Polyimide has good thermal stability and electrospinning can be used to easily control the thickness of the fabricated membrane. Moreover, a new fabrication protocol for ASLBs was proposed that consisted of simultaneously infiltrating the solution of SEs into the assemblies of electrode and SE. One of the challenges for this approach is the low SE filling efficiency because the structure of polyimide nonwoven is relatively closed. Consequently, the voids generated by the low filling efficiency decrease the IC. Another pressing step is suggested to enhance the interconnection between particles inside the template.

Different from the solution infiltration process for preparing sulfide SEs, Nam et al. reported a bendable and thin sulfide electrolyte prepared through mechanically pressing SEs onto a robust template made with poly(paraphenylene terephthalamide) NW.<sup>38</sup> As illustrated in Figure 3C(b), the SEs film was first cast on the Ni film and then transferred into the template by cold pressing. Two configurations of the SE layer (SE–NW–SE and NW–SE–NW) are prepared, and the thickness is as low as 70  $\mu$ m. Because the NW is ion insulating, the ionic conductivities in different configurations vary from 0.16 to 0.34 mS cm<sup>-1</sup>, which are slightly lower than that of pure SEs.

In summary, to deliver cell-level high energy density, the fabrication of a thin solid electrolyte ( $<50 \mu m$ ) is a promising strategy. The conventional slurry coating method to fabricate thin layers may be promising. However, it still faces challenges in the selection of solvent and polymer because of the hypersensitivity of sulfide SEs to polar solvents. The dry method avoids the use of solvents, circumventing this dilemma. While typical binders block ion conduction to some extent, the introduction of ion-conductive binders enhance IC for hybrid electrolyte. Moreover, a thin and robust SE layer can be fabricated by embedding sulfide SEs into the template via the solution or dry method. These processes are promising for reducing thickness but are challenged by unsatisfactory IC. Compared with bulk SE, all of the reported processes utilizing polymeric binders and template increase the mechanical strength of the SE layers but result in ionic conductivities decreasing because of nonionic conductivities and large newborn interface resistance. To overcome these issues, strategies that minimize the amount of binders and ionic conductive binders and templates are suggested for high energy density ASLBs.

2. Cathode Design for High-Energy Sulfide Electrolyte-Based ASLBs. Cathode design plays an important role in developing high energy density ASLBs. Considering the evaluation of battery energy density is based on the capacity and working voltage, the CAM must have high specific capacity and high working voltage. Nevertheless, the delivered energy density in real batteries highly depends on the areal mass loading, and the employment of a thick electrode could effectively minimize the relative volume of inactive materials in total batteries. Benefiting from high transference number  $(\sim 1)$ and high IC, sulfide SEs enable the implementation of thick electrodes. Therefore, the Li ions concentration gradient issue in conventional liquid batteries can successfully be eliminated in ASLBs. In the cathode fabrication processing, it is easy to achieve high areal mass loading in ASLBs through a simple cold pressing approach applied to the mixture of CAM and SEs.<sup>39</sup> However, the performance of a thick cathode is greatly affected by ion and electron transport efficiency. The mixing uniformity of CAM with sulfide SEs and other additives, and the voids and cracks formed inside the cathode layer are crucial

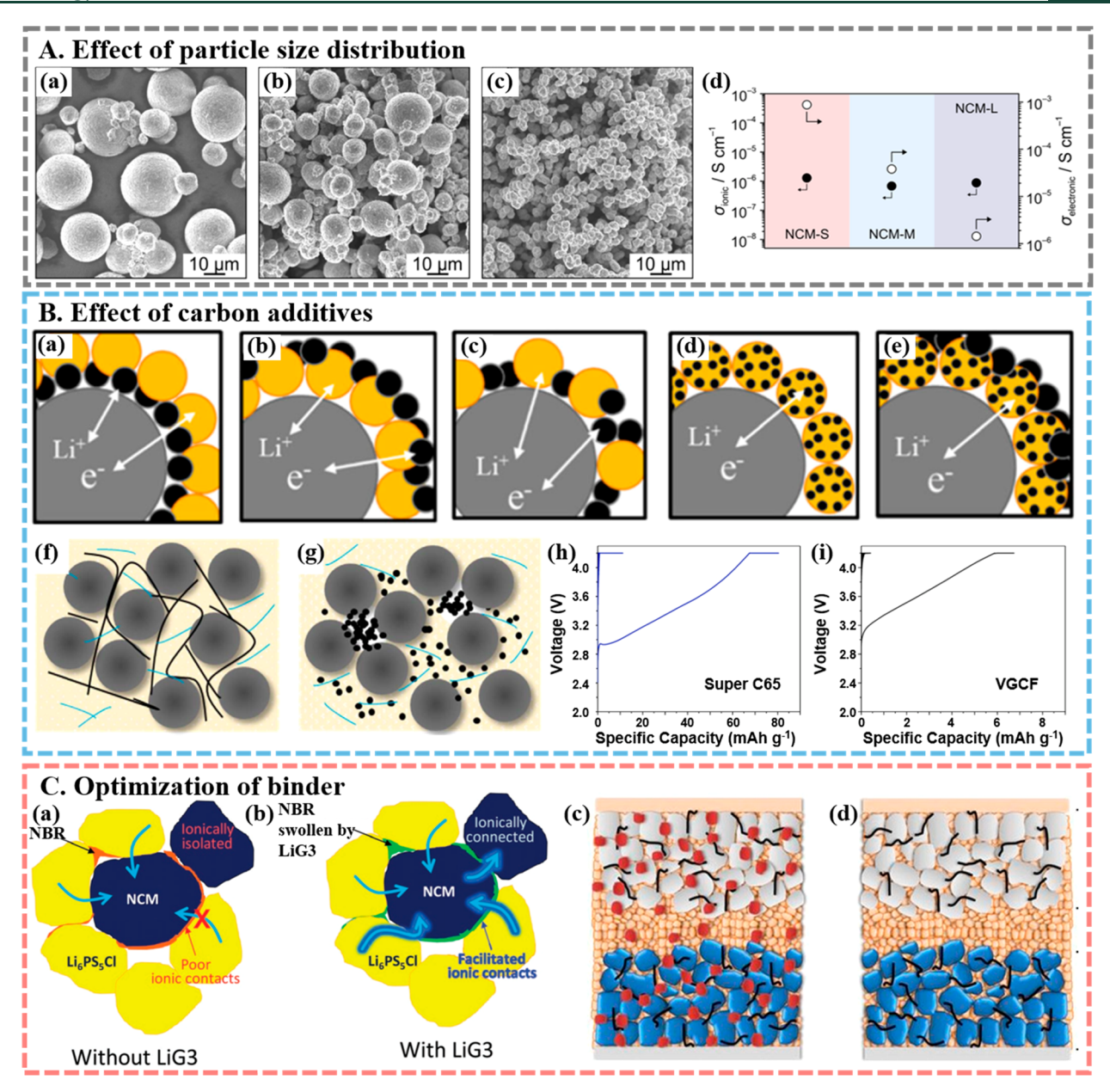


Figure 4. Developing high-voltage cathode based on the optimization in (A) particle size distribution. SEM images of CAM with (a) large, (b) medium, and (c) small size particles. (d) The comparison in ionic/electronic conductivities of cathodes with various sizes of CAM. (Reproduced with permission from ref 47. Copyright 2018 American Chemical Society.) (B) Carbon additives. Protocols of cathodes vary with different carbon and SE locations: (a) carbon at interfacial and SE at interstitial regions, (b) carbon at interstitial and SE at interfacial regions, (c) randomly distributed carbon and SE, (d) both carbon and SE at the interfacial region, and (e) half carbon and SE at interfacial, half carbon at the interstitial region. (Reproduced with permission from ref 50. Copyright 2018 Springer Nature.) Protocols of cathode mixed with (f) VGCF and (g) carbon black, and the effect on SE degradation by introducing (h) carbon black and (i) VGCF. (Reproduced with permission from ref 51. Copyright 2019 Elsevier B.V.) (C) Optimization of the binder. Ion conduction paths in cathode using (a) NBR and (b) NBR swollen by LiG3. (Reproduced with permission from ref 54. Copyright 2019 Wiley VCH.) Scheme of ASLBs (c) before and (d) after removing binder. (S) Reproduced with permission from ref 55. Copyright 2018 Springer Nature.

to the connection and tortuosity, which are related to the efficiency of ionic transport. These issues are related to the cathode designs, including but not limited to the composition of the cathode, the dimensions of CAM and SEs, the ratios and species of carbon additives, the behavior of binders, connections and uniformity of different components, pressure, and more. Meanwhile, the cathode design for different CAM varies. Traditional transition metal oxides, like  $\text{LiCoO}_2$  and  $\text{LiNi}_x \text{Mn}_y \text{Co}_{1-x-y} \text{O}_2$ , are featured with high working voltages, while some Li-free CAM, like S and FeS<sub>2</sub>, are highlighted with

high specific capacities. While there are excellent reviews on high-capacity and high-voltage cathode, 10,40 this section will primarily focus on energy density improvements of ASBL through cathode design optimization based on a classification of high-voltage and high-capacity, including increasing areal mass loading in metal sulfide ASLBs and beyond without sacrificing performance.

2.1. High-Voltage Cathode for High-Energy Density Sulfide Electrolyte-Based ASLBs. Transition metal oxide cathodes, including layered, spinel, and polyanion oxides, are the most

studied high-voltage cathodes. 41 Considering their remarkable gravimetric and volumetric energy density, layered oxides are regarded as the leading candidates for high-energy ASLBs. For example, LiNi<sub>0.8</sub>Mn<sub>0.1</sub>Co<sub>0.1</sub>O<sub>2</sub> delivers a relatively high capacity (>200 mAh  $g^{-1}$ ) and operation voltage (3.8 V), which results in a material-level specific energy of 814 Wh kg<sup>-1,42</sup> However, to fully achieve comparable performance for LIBs with liquid electrolyte, the fraction of CAM in cathode should be further increased. Until now, the CAM loading in most reported ASLBs is around 70 wt %, which is far from the typical 90 wt % in liquid cells.<sup>43</sup> The main challenge is to increase the utilization of CAM. The interface failure with oxide cathodes could be effectively addressed by the interface engineering on CAM, and the interface coating layer can effectively tune the interfacial Li<sup>+</sup> transport kinetics. 13,44-46 Therefore, some issues, like the dimension of electrolyte and CAM, distribution and morphologies of carbon additives, and optimization of binders are introduced in this section.

2.1.1. Dimension of Electrolyte and Cathode Active Materials. The dimension of CAM and SEs significantly impacts the performance of ASLBs. Typically, sulfide SE-based cathode in cold-pressed ASLBs is composed of only CAM and SEs to avoid degradation of SEs caused by carbon additives. The total electron and ion conductions are derived from the CAM and SEs, respectively. Therefore, the effective percolations of CAM and SEs are essential to provide sufficient electron and ion transport, especially in a cathode with high mass loading. In this case, the particle size distributions of CAM and SEs are very important.

Starauss et al. investigated the effect of CAM particle size on the performance of ASLBs (Figure 4A).<sup>47</sup> Three types of NMC with average particle sizes of 15.6, 8.3, and 4.0  $\mu$ m are selected as large, medium, and small CAM (Figure 4A(a-c)), respectively, and  $\beta$ -Li<sub>3</sub>PS<sub>4</sub> acted as the sulfide SE. It is impressive that NMC with a smaller size exhibited much better performance, such as higher specific capacity and lower overpotential. Through an ex situ XRD measurement, the existence of electrochemically inactive CAM was confirmed in all three groups of samples, and their fraction largely depended on the particle size. The effect of particle size on mean electronic conductivity and IC of the total electrodes (CAM/ SE) is investigated (see Figure 4A(d)). Compared with the invariable IC, the electronic conductivity decreased by 3 orders of magnitude for large particles, which is attributed to the presence of fewer contact points and thereby insufficient pathways for electron conduction. In addition, the particle size of SE affects the performance of ASLB. Shi et al. investigated the effect of particle size ratio of CAM to SEs ( $\lambda$ ) on ASLBs with high mass loading.<sup>43</sup> The SE particle size is suggested to be smaller than that of CAM particles, and the  $\lambda$  needs to be further enhanced when increasing the volume loading of CAM. The utilization of CAM is improved from 20% to 100% when SE particle size was reduced by a factor of 2-3 that of the cathode. The optimized performance is achieved when  $\lambda$  was the highest (CAM with 12.5  $\mu$ m and SE with 1.5  $\mu$ m), which was confirmed both computationally and experimentally.

It should be noted that the aforementioned dimension of CAM is based on the polycrystalline structure, where the grain boundaries between crystals may impede the ion diffusion. Wang et al. reported that single-crystal  $\text{Li}(\text{Ni}_{0.5}\text{Mn}_{0.3}\text{Co}_{0.2})\text{O}_2$  exhibited higher capacity and better rate performance than polycrystalline cathode in ASLBs, which was attributed to the 6–14 times higher  $\text{Li}^+$  diffusion coefficient in single-crystal

cathode materials.<sup>48</sup> This result indicated that the single-crystal cathode had great potential for developing a thick cathode laver.

2.1.2. Distribution and Morphology of Carbon Additives. Introducing carbon additives to the cathode is an effective method to enhance the electric conductivity in the total electrode. As aforementioned, the electron conduction in cathode is derived from the intrinsic electrical conductivity of CAM. Though good capacity has been achieved, the ASLB delivers an unsatisfactory rate performance, which is highly restricted by the electrical conductivity. Carbon is usually considered as a leading option for batteries. However, the enhanced electrical conductivity accelerates the decomposition and negatively affects the electrode performance of sulfide SEs at high voltages, because of the narrow ESW of sulfide SEs (1.7–2.3 V). Therefore, it is important to optimize the carbon loading. The performance is also affected by the mixing approaches and species of carbon additives, shown in Figure 4B.

Noh et al. reported the influence of the location of carbon on the cathode, which causes the mixing method to dramatically impact the performance. The authors proposed a total of five mixing protocols to control the position of carbon and evaluated the corresponding electrochemical performance, as illustrated in Figure 4B(a-e). The particle location is controlled based on the principle that the first two powders that are mixed have the most intimate contact, while the third powder will present in the interstitial regions. In their work, the carbon at the interfacial and interstitial regions determined the interfacial and percolation conductivities, respectively. As a result, the protocol (Figure 4B(e)) that led to carbon being present not only at the CAM interfaces but also at the interstitial regions between CAM and SEs delivered high initial capacity and good rate performance.3D conducting

3D conducting networks can provide the capability for sufficient electron conduction but with less contact area with sulfide SEs, which is favorable to improve the performance of all-solidstate batteries employing a thick cathode layer.

networks can provide the capability for sufficient electron conduction but with less contact area with sulfide SEs, which is favorable to improve the performance of all-solid-state batteries employing a thick cathode layer.

Various carbon species were investigated by Ates et al., shown in Figure 4B(f-i). Carbon black is one of the most common conductive additives in LIBs. It features a morphology with primary particles of a few nanometers agglomerated to size larger than 100 nm. Because of the large size difference from CAM and SEs, homogeneous mixing of carbon was achieved to provide paths for electrons conduction, which benefits the reaction kinetics of CAM. However, the increased interfaces between carbon and SEs accelerate the decomposition of the SEs (Figure 4B(h)). Therefore, vapor growth carbon fiber (VGCF), which has 1D morphology, is frequently used in sulfide-based ASLBs. The percolation of the 1D fibers provides sufficient electron conductivity and minimizes the adverse effect due to the decreased exposure

to SEs (Figure 4B(i)). Moreover, the employment of VGCF also leads to lower empty volume compared to carbon black nanoparticles. However, it is inevitable that there are still side reactions between carbon and sulfide SEs. Deng et al. reported that the introduction of a semiconductive additive, poly(3,4-ethylenedioxythiophene) (PEDOT), could effectively eliminate the detrimental effects of carbon nanotubes and enhance the electron transfer. <sup>52</sup>

2.1.3. Optimization of Binders. The binder is a significant factor for scaling from laboratories to commercialization for ASLBs. The typical fabrication process of the cathode in labscale sheet-type ASLBs is casting cathode powder onto the cold-pressed electrolyte layer followed by pressing. Preparing a cathode layer and then pressing with the SE layer and anode is another approach, where polymeric binders are essential. Binders help the cathode maintain mechanical strength for fabrication, adhere particles, and buffer the volume change of CAM. 53 As aforementioned, there are various limitations to the introduction of polymers in sulfide SEs. Furthermore, the binder loading needs to be optimized because these molecules increase cell impedance by blocking both ion and electron conduction. The desired properties for binders are good binding effect, low weight fraction, and minimal effect on ion conduction, which are very critical to a high mass loading cathode.

To eliminate the negative effect caused by solvent, Hippauf et al. developed a dry-film process to fabricate cathode sheets using polytetrafluoroethylene (PTFE) as a binder.<sup>53</sup> PTFE is chosen because of its high chemical and electrochemical stability. More importantly, under a shear force, the PTFE beads are transferred into nanoscale fibrils, which increases PTFE's binding effect. In their work, flexible and freestanding NMC sheets with a thickness of 97  $\mu$ m and an area of 9 cm<sup>2</sup> were obtained with a reduction in the binder loading to 0.1 wt %. The fraction of CAM in this composite cathode is as high as 85 wt %, and the sheets featured a high areal loading of 6.5 mAh cm<sup>-2</sup>. It should be noted that the rate performance slightly decreased because of the amount of binder, which may be explained by the PTFE's inability to conduct ions, poor electronic conductivity, and insufficient ion conduction due to a low ratio of SEs.

Therefore, utilizing binders that conduct ions is a good strategy to balance the negative effect on IC, as illustrated in Figure 4C(a,b). Oh et al. reported a slurry fabrication protocol for sheet-type ASLBs using a Li ion conductive polymeric binder, which was the combination of NBR with solvate ionic liquids (LiG3, G3 is triethylene glycol dimethyl ether).<sup>54</sup> To circumvent the undesired side reactions and phase separation between solvent, binders, and sulfide SEs, dibromoethane, a solvent with intermediate polarity, was chosen for the preparation of the slurry. In addition to the thin SE layers (70  $\mu$ m), a cathode layer with ultrahigh mass loading (45 mg<sub>CAM</sub> cm<sup>-2</sup>) and a high fraction of CAM (≥80 wt %) was fabricated. Compared with using only non-IC NBR as a binder, this ionic conductive binder increased capacities from 144 to 174 mAh  $g^{-1}$  for LiNi<sub>0.6</sub>Mn<sub>0.2</sub>Co<sub>0.2</sub>O<sub>2</sub> and 76 to 160 mAh  $g^{-1}$  for Li<sub>4</sub>Ti<sub>5</sub>O<sub>12</sub>, resulting in a high areal capacity of 7.4 mAh cm<sup>-2</sup> for LiNi<sub>0.7</sub>Mn<sub>0.15</sub>Co<sub>0.15</sub>O<sub>2</sub>. The additional ion-conduction path provided by conductive binders is confirmed by <sup>7</sup>Li nuclear magnetic resonance (NMR), explaining the enhanced electrochemical performance.

To eliminate the negative effect brought by binders, Yamamoto et al. reported a binder-free strategy by removing the volatile binder after the fabrication of ASLBs (Figure 4C(c,d)). In a slurry coating process, poly(propylene carbonate) (PPC)-based binders and nonpolar anisole solvent are utilized. The anisole dissolves the PPC and is stable with sulfide SE ( $75Li_2S\cdot25P_2S_5$ ). More impressively, the PPC thermally depolymerizes and evaporates at a temperature below 300 °C, which produces binder-free ASLBs. While the IC of PPC-contained SE ( $1.1 \times 10^{-4}$  S cm<sup>-1</sup>) was lower, the IC of PPC-removed SE was consistent with the value of pristine SE ( $4.1 \times 10^{-4}$  S cm<sup>-1</sup>). As a result, binder-free ASLBs exhibited enhanced rate performance and cycling stability with a cell-level energy density of 115 Wh kg<sup>-1</sup>.

2.2. High-Capacity Sulfur-Based Cathode for High Energy Density Sulfide Electrolyte-Based ASLBs. Compared with oxide cathodes that deliver high voltage but low capacity, sulfide cathodes, especially elemental sulfur and Li2S, exhibit extremely high capacity (1675 mAh g<sup>-1</sup> for S and 1170 mAh  $g^{-1}$  for Li<sub>2</sub>S) and a moderate working voltage (~2.1 V), which enables ASLBs with a theoretical energy density as high as 2600 Wh kg<sup>-1</sup>.<sup>10,56</sup> Pairing sulfide SEs with sulfide cathode shows the potential to provide higher energy density than conventional LIBs. The first benefit of sulfide SEs is the suppression of the polysulfide shuttle effect which widely exists in batteries using the liquid electrolyte and causes a loss of active material. The second benefit is that sulfide SEs are fireresistant, meaning they help quell safety concerns about short circuits caused by Li dendrites. Third, sulfide cathodes have high chemical compatibility with sulfide electrolyte, meaning the extra coating layers on oxide cathodes are circumvented. Further, the working voltage range of sulfide cathodes matches well with the ESW of sulfide SEs, which enables a highly stable cycling performance.

To meet the goals (500 Wh kg<sup>-1</sup> in gravimetric energy density), Yang et al. proposed key parameters for the cathode, such as sulfur content >50 wt %, sulfur loading of 4-6 mg cm<sup>-2</sup>, specific capacity of 1200 mAh g<sup>-1</sup>, and cathode porosity <15-20%. 10 Unfortunately, no published work has reported reaching these values. Ignoring the effect of the SE layer, the main shortcoming is the low utilization of high mass loading CAM in the cathode layer. The dilemma is related to not only the poor ion and electron conduction paths but also to the sluggish activation of CAM during electrochemical reactions. Whereas oxide SEs have considerable electron conductivity, sulfur is electrically insulating (electrical conductivity:  $10^{-30}$  S cm<sup>-1</sup>), which causes a great challenge for the electrode design. More conductive additives are necessary to provide effective percolation, which inevitably reduces the ratio of CAM in the total electrodes. Meanwhile, the poor ion transport across the CAM and SE interface appears to be the performance's bottleneck.<sup>57</sup> In addition, there is an 80% volume change during the conversion between S and Li<sub>2</sub>S, which causes severe delamination of CAM and impedes ion/electron networks. The decreasing utilization of CAM causes the fast decay of cycling performance. Even so, various strategies that enhance the utilization of sulfur, such as improving the ion/electron accessibility to CAM, enhancing the ion/electron conductivities of CAM, confining the volume change, and so on, are summarized to inspire more advances toward cell-level highenergy ASLBs.

2.2.1. Improving Ion and Electron Accessibility for Cathode Active Materials. To achieve high energy density, highly efficient ion and electron accessibility to CAM are critical for ASLBs. Generally, in the cathode layer, percolated carbon

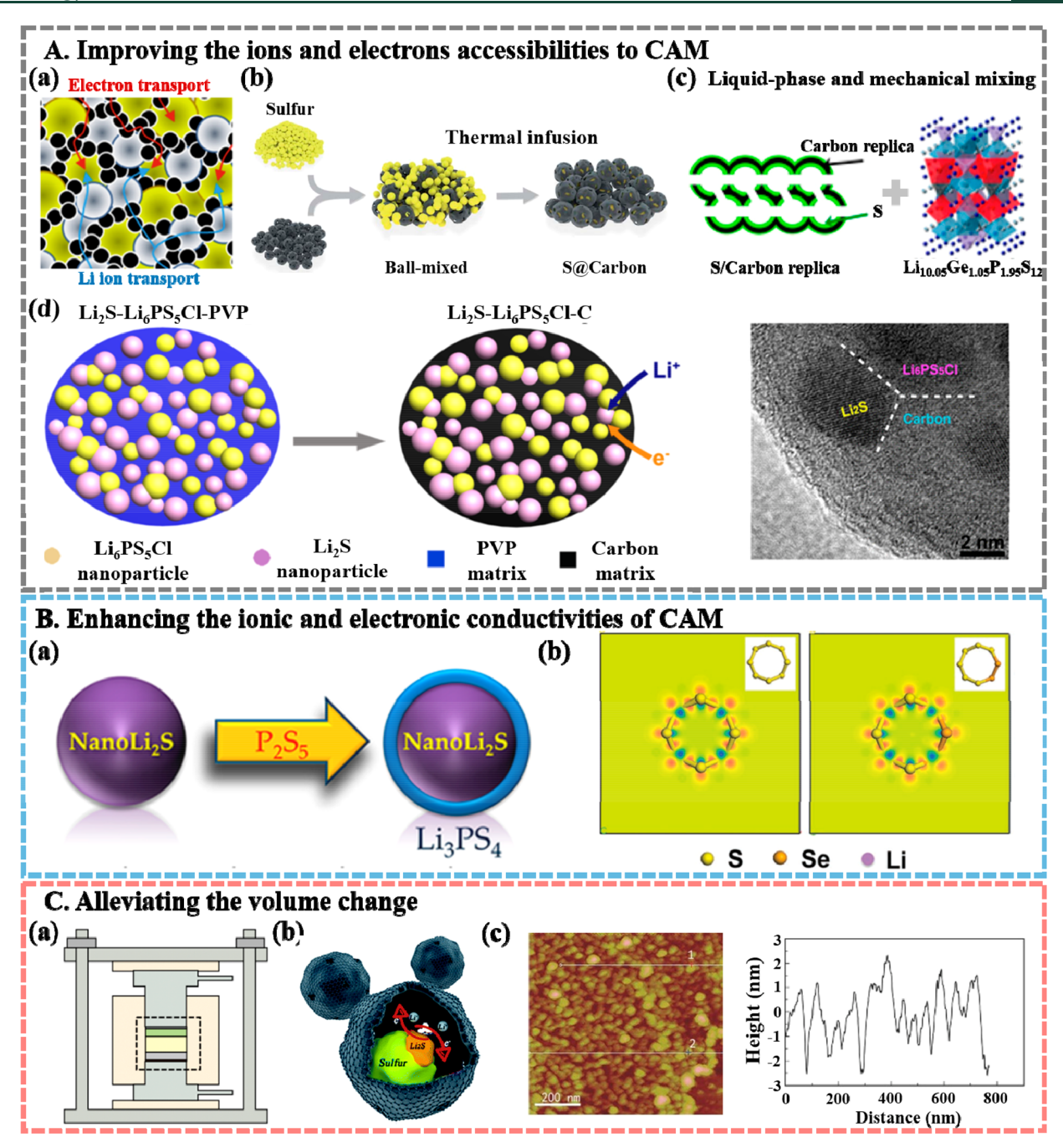


Figure 5. Developing high-energy sulfide-cathode-based ASLBs through (A) improvement in ions/electrons accessibility to CAM. Schematic of the cathode (a) with efficient ion/electron conduction paths<sup>58</sup> (Reproduced with permission from ref 58. Copyright 2017 Elsevier B.V.) and fabricated routes through (b) thermal<sup>60</sup> (Reproduced with permission from ref 60. Copyright 2019 Royal Society of Chemistry.), (c) liquid-phase and mechanical mixing<sup>61</sup> (Reproduced with permission from ref 61. Copyright 2018 American Chemical Society.), and (d) in situ synthesis approaches.<sup>63</sup> (Reproduced with permission from ref 63. Copyright 2016 American Chemical Society.) (B) Enhancement in ionic/electronic conductivities of CAM. (a) Schematic of the fabrication of Li<sub>2</sub>S@Li<sub>3</sub>PS<sub>4</sub> core—shelled structure.<sup>64</sup> (Reproduced with permission from ref 64. Copyright 2013 American Chemical Society.) (b) Electron densities of S<sub>8</sub> and Se<sub>2</sub>S<sub>6</sub> rings.<sup>65</sup> (Reproduced with permission from ref 65. Copyright 2019 Wiley VCH.) Alleviation of the volume change. Schematic of (a) the pressurized cell and (b) the Li<sub>2</sub>S@Carbon core—shelled structure.<sup>60</sup> (Reproduced with permission from ref 60. Copyright 2019 Royal Society of Chemistry.) (c) Atom image of amorphous rGO@S and corresponding height profiles at line 1.<sup>69</sup> (Reproduced with permission from ref 69. Copyright 2017 Wiley VCH.)

additives and SEs are introduced to construct electron and ion conduction paths, respectively, and intimate contacts in CAM are necessary to boost the electrochemical reaction (Figure 5A(a)). S8

Mechanical mixing is one of the most widely used methods to blend the CAM with both SEs and carbon additives homogeneously. By enhancing the mixing intensity and prolonging the mixing time, the mixing uniformity can be greatly improved. The morphology, particle size, and even crystallinity can be considerably affected during these processing steps. Nagao et al. compared the performance of S-based cathodes mixed through mortar grinding (low-energy)

and ball milling (high-energy) methods. 59 The mixing caused a reduction in particle size, and amorphization of sulfur induced and improved contact between the molecules, which contributed to more sufficient electron and ion transport pathways. As a result, the ball-milled samples exhibit better performance. Additionally, given sulfur's low melting point (112 °C), mixing components at high temperature or further heat treatment after mixing are beneficial for creating intimate contact between sulfur and carbon. As shown in Figure 5A(b), Han et al. reported a melting diffusion approach for mixing sulfur and mesoporous carbon with interconnected pores at 155 °C, which exhibited a high capacity of 1391.3 mAh g<sup>-1</sup> after 1200 cycles at a high current rate of 0.2 C.60 This improved result was attributed to the core-shelled structure, which effectively enhanced the electrical conductivity and decreased the ohmic polarization. Further, to enhance the ions accessibility to the sulfur inside the mesopores, Suzuki utilized the capillary effect to infiltrate the pores with liquid phase sulfide SEs (Figure 5A(c)), which led to comparable cycling performance to that of a battery with liquid electrolyte.<sup>6</sup>

Compared with cathode fabricated by mixing all of the components, the *in situ* synthesis method generates a more uniform mixture and intimate contact in the cathode. Yan et al. reported an *in situ* approach where Li<sub>2</sub>S/C nanocomposite was generated by the combustion of Li metal in CS<sub>2</sub>.<sup>62</sup> The nanosized Li<sub>2</sub>S is uniformly embedded in the conductive carbon matrix, which improves the electron conductivity and effective confinement on volume change. Han et al. reported an ingenious strategy for homogeneous nanocomposite cathode preparation where nanoparticles of Li<sub>2</sub>S and Li<sub>6</sub>PS<sub>5</sub>Cl were uniformly confined in a nanoscale carbon matrix through a coprecipitation and high-temperature carbonization process, as illustrated in Figure 5A(d).<sup>63</sup> This special design enabled simultaneously enhanced ion and electron conductivities and ASLB with high utilization of CAM (71%).

2.2.2. Enhancing the Ionic and Electronic Conductivities of Cathode Electrode. Besides improving the ion/electron accessibility, the enhancement of ionic and electronic conductivities is an effective approach to boost the utilization of CAM. The material dimensionality and defect significantly impact ion conduction capability. Lin et al. reported that nanoparticles of Li<sub>2</sub>S exhibited an IC 2 orders of magnitude higher than bulk Li<sub>2</sub>S due to the reduced particle size and increased defects. 64 As illustrated in Figure 5B (a), the IC of Li<sub>2</sub>S was greatly increased from 10<sup>-11</sup> to 10<sup>-7</sup> S cm<sup>-1</sup> by in situ forming Li<sub>3</sub>PS<sub>4</sub> core-shelled structures (Li<sub>2</sub>S@ Li<sub>3</sub>PS<sub>4</sub>). The contact area between Li<sub>2</sub>S and Li<sub>3</sub>PS<sub>4</sub> is increased, which is crucial to obtain higher utilization of CAM. In addition, Li et al. favorably tailored both ionic and electronic conductivities of SeS<sub>x</sub>-Li<sub>3</sub>PS<sub>4</sub>-C cathodes by tuning the ratio of Se to S in the solid solution of SeS<sub>x</sub>.<sup>65</sup> As illustrated in Figure 5B(b), the Se substitution in the  $S_8$  ring (ortho- $Se_2S_6$  is the example here) increased the density of states in the electronic structure of S atoms, which led to an increase in electron densities per S atom and correspondingly enhanced electronic conductivities. Moreover, an interaction between SeS<sub>x</sub> and Li<sub>3</sub>PS<sub>4</sub> is proposed to explain the improvement in both ionic and electronic conductivities. Zhang et al. reported an acceleration in the reaction kinetics by introducing Se into S cathode. 66 It should be noted that the capacity of CAM was decreased to some extent owing to the introduction of the additives, suggesting that the balance between capacity and reaction kinetics is crucial to achieving targeted goals.

2.2.3. Alleviating Volume Changes. Electrode volume change during lithiation/delithiation is a common challenge for batteries and is even more severe for high-capacity electrodes (volume changes of up to 80% for S).<sup>67</sup> The resulting strain from volume change may cause cracks and delamination of the CAM to SE interface, which hinders the long-term cycling performance. To stabilize cycle life of an ASLB using sulfur cathode, it is crucial to alleviate stress/strain caused by volume change during cycling. Applying external pressure during the cell operation, referred to as operating pressure, on the ASLBs is widely used when employing sulfide SEs, as illustrated in Figure 5C (a). The external pressure confines the CAM to a limited space and maintains intimate contact between various components. However, the relationship between operating pressure and cycling stability for ASLB using S cathode is not clear, though Doux et al. have shown that this pressure has a low influence on cycling stability for oxide cathodes when at a reasonably low value (50 MPa).<sup>68</sup> In addition to external pressure, a specialized cathode design could alleviate the volume change to some extent. As shown in Figure 5C (b), embedding nanoparticles of S into a porous carbon matrix, like the core-shelled structure, could effectively buffer the volume change.<sup>60</sup> Yao et al. reported that a conformal coating of amorphous S onto reduced graphene oxide (labeled as rGO@ S) could reduce the interface resistance and stress/strain generated by volume change. 69 The thickness of the amorphous sulfur layer was only 2 nm, as depicted in Figure 5C (c), which contributed to a uniform volume change.

In summary, to successfully develop high-energy ASLBs using high-voltage cathodes, the challenge of insufficient electron conductivity in thick electrodes must be overcome. The narrow ESW of sulfide SEs limits the use of carbon additives at high voltage. Even though the optimization of carbon additives and particle size distribution of CAM and SEs effectively alleviate the poor electron conduction, the poor ion conductivity has yet to be overcome for a practical application of thick electrodes. Therefore, special cathode designs are necessary to balance the degradation of sulfide SEs and enhance electron conductivity. The proposed 3D conducting networks can provide sufficient electron conduction but less contact area with sulfide SEs, which is favorable for improving battery performance. Additionally, it is a promising approach to construct a composite electrode configuration with wide ESW electrolytes, such as halides. Compared with oxide cathodes, sulfide-based cathodes possess higher capacity and have more compatible interfacial stability with metal sulfide SEs. However, sulfide-based cathodes have poor ion and electron accessibility, which significantly affects the ratio of CAM in total electrodes and reaction kinetics. Uniform mixing of different components is necessary to provide sufficient ion and electron conductive paths, and the amount of inactive materials should be further decreased to lower than 40%. Lastly, another challenge is the volume expansion of sulfidebased cathodes.

3. Li Metal Anode Design for High Energy Density Sulfide Electrolyte-Based ASLBs. Among various anode candidates, Li metal has become one of the most promising anodes for high-energy ASLBs because of its high theoretical special capacity and lowest redox potential. However, Li metal still faces several challenges in developing cell-level high-energy ASLBs. First, excess Li is often used in ASLBs, which limits the energy density. Moreover, owing to the severe reaction of sulfide SEs against Li metal, the interface stability between

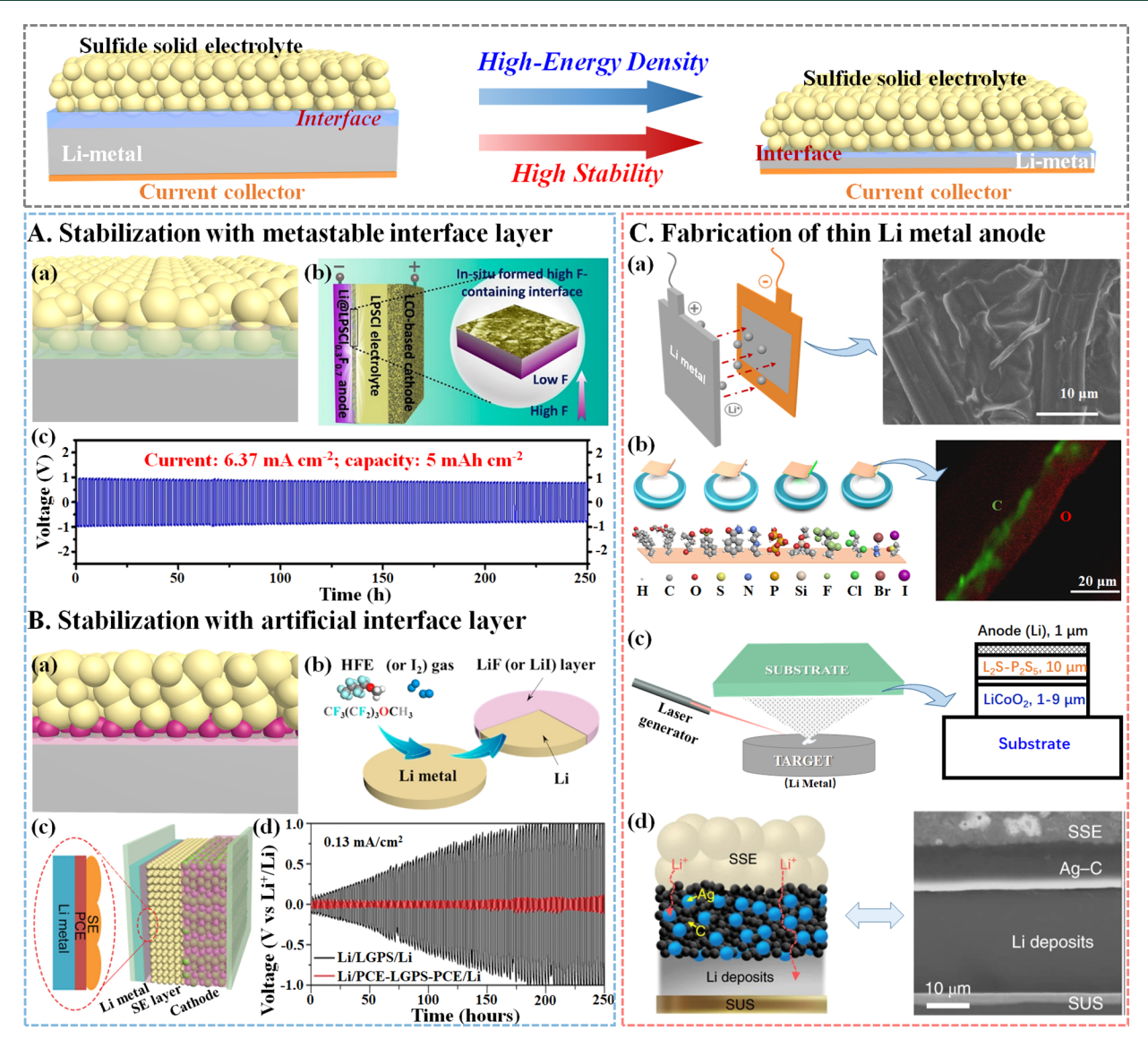


Figure 6. Li-anode configuration design and interface stability strategies for high energy density in ASLBs (top scheme): (A) (a) metastable interphase generated through sulfide SEs side reaction with Li metal; (b) schematic diagram of the Li@LPSCl<sub>0.3</sub>F<sub>0.7</sub>//LPSCl//LCO@LNO/LPSCl ASLBs with the highlighted interface layer. (Reproduced with permission from ref 73. Copyright 2020 American Chemical Society.) (c) Li plating and stripping in Li//LPSCl<sub>0.3</sub>F<sub>0.7</sub>//Li symmetric cells at current density of 6.37 mA cm<sup>-2</sup> and cutoff capacity of 5 mAh cm<sup>-2.73</sup> (Reproduced with permission from ref 73. Copyright 2020 American Chemical Society.) (B) (a) Artificial interphase introduced between Li metal sulfide SEs; (b) schematic diagram of the process for the surface coating of LiF (or LiI) layers on the Li metal surface <sup>74</sup> (Reproduced with permission from ref 74. Copyright 2018 Elsevier B.V.); (c) schematic diagram of ASLBs with the PCE interlayer; (d) overpotential of the Li<sup>+</sup> platting/stripping of Li/LGPS/Li and Li/PCE-LGPS-PCE/Li at 0.13 mA cm<sup>-2.77</sup> (Reproduced with permission from ref 77. Copyright 2019 Wiley VCH.) (C) (a) Electrochemical predeposition strategy for thin Li anode fabrication (left) and SEM images of CFC/G/ZnO current collector plated with Li (right). (Reproduced with permission from ref 80. Copyright 2018 Elsevier B.V.) (b) Schematic of an ultrathin Li layer formed onto lithiophobic substrates (left) and Elemental distribution image of C and O on the ultrathin Li (right). (Reproduced with permission from ref 81. Copyright 2019 Springer Nature.) (c) The ultrathin Li anode by pulsed laser deposition (PLD) (left) and schematic cross-sectional view of the thin-film battery (right). (Reproduced with permission from ref 86. Copyright 2012 Elsevier B.V.). (d) Silver–carbon composite Li-free anodes (left) and pristine cross-sectional SEM image for the Ag-C nanocomposite layer (right). (Reproduced with permission from ref 27. Copyright 2020 Springer Nature.)

sulfide SEs and Li metal anode needs to be further improved. Meanwhile, Li dendrite growth in sulfide SEs negatively affects the battery cycling life, Coulombic efficiency, energy density, and safety. Because we have systematically summarized the Li growth mechanisms, suppression strategies, and characterizations in ASLBs in our previous review, the discussion on Li dendrites will not be included in this Review. In this section, we summarize some strategies for the stabilization of the interface between sulfide SEs and Li metal anodes and

approaches in the development of thin Li and even anode-free methods, which improves cycling stability and energy density of ASLBs for practical application (see top scheme in Figure 6). A thin Li metal anode and even anode-free methods are promising strategies to enhance the energy density of ASLBs. In sulfide-based ASLBs, constructing a stable interphase is very important to achieve excellent battery performance.

A thin Li metal anode and even anodefree methods are promising strategies to enhance the energy density of ASLBs. In sulfide-based ASLBs, constructing a stable interphase is very important to achieve excellent battery performance.

3.1. Interface Stabilization between Li Metal and Sulfide Solid Electrolytes. Interface stability is one of the most critical issues when pairing sulfide SE with Li metal. In ASLBs, the deposition/dissolution of Li metal occurs only at the solidsolid interface between Li metal and sulfide SEs. However, most sulfide SEs are electrochemically and chemically unstable in the presence of Li metal, resulting in the formation of an interphase layer with high resistance. Therefore, it is crucial to stabilize the interface between Li metal and sulfide SEs to achieve excellent battery performance. The introduction of an interface protective layer with high stability and ion conductivity could effectively inhibit the sulfide decomposition and reduce ion conduction resistance. Considering the difference in origins, two main strategies of interface layer modification are detailed in this section: (1) a metastable interphase generated through the reaction of sulfide SEs and Li metal (see Figure 6A (a)) and (2) an artificial interphase introduced through modifying Li metal surface or adding an additional layer between SEs and Li metal (see Figure 6B (a)).

3.1.1. Interface Stabilization through the Formation of Metastable Interphase. It is a promising design to form a metastable interphase to stabilize the interface between Li metal and SEs. As aforementioned, an interphase can be formed between Li metal and sulfide SEs by reaction with Li metal, whose composition highly determines the conductivity and stability for the two layers contact. For example, the Li-P-S SEs decompose to Li<sub>2</sub>S, P<sub>4</sub>S<sub>9</sub>, and Li<sub>3</sub>P by reacting with Li metal. These products generate a stable interface with good IC and low electronic conductivity between Li metal and sulfide SEs. 70 In contrast, an unstable interphase was found in sulfide SEs containing Ge, such as Li<sub>10</sub>GeP<sub>2</sub>S<sub>12</sub> (LGPS), LiGeS<sub>4</sub>, and Li<sub>3.25</sub>Ge<sub>0.25</sub>P<sub>0.75</sub>S<sub>4</sub>. The interphase with mixed ionic and electronic conductivities induced new Li deposition at the interface with SE, which caused decomposition of SE and thereby resulted in the continuous corrosion of the bulk sulfide SEs. 7051 Therefore, it is promising to stabilize the interface by adjusting the interphase composition through the reaction of SEs and Li metal.

The interphase containing Li halides, especially LiF and LiI, are proposed to stabilize the interface, because their lower Li<sup>+</sup> diffusion energy and high surface energy favor the enhancement of Li<sup>+</sup> surface diffusion and stabilization of SE in Li plating/stripping. Wang's group and Sun's group reported a strategy to establish a stable protective layer containing LiI and LiF by the reaction between halide-doped sulfide SEs and Li metal, respectively. As illustrated in Figure 6A (b), fluorinated argyrodite Li<sub>6</sub>PS<sub>5</sub>Cl (LPSCl<sub>0.3</sub>F<sub>0.7</sub>) was employed to *in situ* generate a condensed and highly fluorinated layer at the interface between Li metal and sulfide SEs. As a result, a superstable Li plating/stripping cycling in the symmetric cell was achieved at an ultrahigh current density of 6.37 mA cm<sup>-2</sup> and a cutoff capacity of 5 mAh cm<sup>-2</sup> (Figure 6A (c)).

3.1.2. Interface Stabilization through the Introduction of Artificial Interphase. Moreover, in addition to the in situ introduction of a metastable interphase, the formation of an artificial interface layer is also an effective method to stabilize the interface between Li metal and sulfide SEs, which is widely applied for oxide SEs. An artificial interface layer (ex situ) can be established on the surface of Li metal by introducing an additional protective layer or reacting Li metal with specific chemicals, which must have excellent chemical stability with both sulfide SEs and Li metal, high ion conductivity, and appropriate mechanical strength. Pretreatment on Li metal is a widely used strategy to introduce this interface layer. Wang et al. reported an approach that the LiF or LiI interfacial layer could be formed by reacting Li metal with CF<sub>3</sub>(CF<sub>2</sub>)<sub>3</sub>OCH<sub>3</sub> or I<sub>2</sub> (gas) (Figure 6B(b)).<sup>74</sup> The SEM morphologies of LiF and LiI on the surface of Li metal were different. LiI has a rougher and more porous surface, while LiF has a denser surface. As a result, compared to a symmetric cell using bare Li metal, both LiF and LiI-coated Li metal symmetric cells showed more stable cycling at 0.1 mA cm<sup>-2</sup>. While at a higher current density (0.5 mA cm<sup>-2</sup>), the symmetric cell assembled with a LiF-modified Li metal remained stable with a low overpotential in the entire 200 cycles. In contrast, the LiI-coated symmetric Li metal cell showed a short circuit after 150 cycles. To further achieve an adjustable protective layer on the surface of Li metal, Sun et al. reported an in situ and self-limiting reaction where P<sub>4</sub>S<sub>16</sub> is reacted with Li metal in N-methyl-2-pyrrolidone (NMP).<sup>75</sup> An interfacial layer of Li<sub>3</sub>PS<sub>4</sub> with high ion conduction was formed on the surface of Li metal, in which the thickness of Li<sub>3</sub>PS<sub>4</sub> can be adjusted by controlling P<sub>4</sub>S<sub>16</sub> concentration in NMP. The symmetric cell with the Li<sub>3</sub>PS<sub>4</sub> protective layer enabled it to deliver a stable Li stripping and plating process for 2000 h at 0.5 mA cm<sup>-2</sup> and 1 mAh cm<sup>-2</sup> capacity.

In addition, atomic layer deposition (ALD), which is a conventional thin-film coating method, is employed to stabilize the interface between Li metal and sulfide SEs. Gewirth and co-workers fabricated an ultrathin  $Al_2O_3$  interlayer (thickness of 10 nm) on the surface of Li metal by ALD to enhance interface stability between Li metal and sulfide SEs. The  $Al_2O_3$  layer was converted to  $Li_xAl_{(2-x/3)}O_3$  by the reduction of Li metal, which not only was favorable to  $Li^+$  conduction but also suppressed the interfacial reaction between Li metal and sulfide SEs ( $Li_7P_3S_{11}$ ). As a result, the cycling number was dramatically increased for Li symmetric cells.

On the other hand, the stable interface layer with both SEs and Li metal can be directly introduced. Sun et al. reported a succinonitrile (SN)-based plastic crystal electrolyte (PCE) as interphase to prevent interfacial issues (Figure 6B(c)). As shown in Figure 6B(d), the Li/PCE-LGPS/Li symmetric cell showed stable overpotential at 0.13 mA cm $^{-2}$  for 250 h. The overpotential of the Li/LGPS/Li symmetric cell gradually increased with increasing time at the same conditions, suggesting that the PCE interlayer stabilized the interface between Li metal and sulfide SE. In addition, the glass material containing Li<sub>2</sub>S-P<sub>2</sub>S<sub>5</sub>-P<sub>2</sub>O<sub>5</sub> was also reported as an interface layer to stabilize the interface between Li metal and LGPS in Li–S solid-state battery.  $^{69}$ 

In summary, the interface instability with sulfide SEs is the major obstacle in the utilization of Li metal anode. The formation of a metastable interphase and the introduction of an artificial layer on the surface of Li metal and sulfide SEs are effective strategies to stabilize the interface between Li metal

and sulfide SEs and result in excellent battery performance. The formation of a metastable interphase needs special electrolyte composition, such as halide substitutions, which may limit the design of sulfide SEs. Forming a metastable interphase requires a rest process after cell assembly or the cell must be precycled, which is time- and/or energy-consuming. In contrast, the artificial layer strategy is flexible and feasible. For Li metal surface modification strategies, ultrathin artificial layers are generated, which minimally affects energy density. However, the introduction of an additional interlayer (commonly the thickness at hundreds of micrometers) may increase the gross mass of the cell, which is harmful to the improvement of energy density. In addition, considering the rigid contact at the interface, the mechanical stability of this interface layer is critical to effectively suppress the dendrite growth, which lacks investigation until now.

3.2. Thin Li Metal and Anode-Free Configurations in ASLBs. After the interface between Li metal and sulfide SEs is stabilized, a thin Li metal anode is suggested to boost the energy density of ASLBs. Conventional Li foil used in ASLBs has a thickness of over 200  $\mu$ m, which is excessive for practical application and limits the energy density at the cell level. In order to improve energy density, the anode needs to minimize the amount of Li metal in ASLBs by designing a thin Li metal anode (<50  $\mu$ m) or even a Li-free anode. In this section, some strategies, like roll-to-roll extrusion, electrochemical plating, thermal infusion, pulsed laser deposition (PLD), and vacuum thermal vapor deposition (VTVD), are introduced separately to construct thin Li anodes in ASLBs. Further, the anode-free design is also discussed.

Considering the good ductility of Li metal, the most direct way to fabricate thin Li metal anodes is by using mechanical compressing, such as roll-to-roll extrusion. The thickness of Li metal foil mainly results from the pressure exerted by the holding extension applied to Li metal at the inlet of the roller mill and the process unwinding speed. Generally, the thickness of the Li anode prepared by roll-to-roll manufacturing can be controlled from 5 to 100  $\mu$ m. However, the fabrication of a defect-free thin Li metal foil is still challenging because of Li metal's strong adhesion.

Electrochemical deposition is a common and feasible approach to construct a metal film on current collectors, which is also available to prepare thin Li metal film. Liu et al. designed and fabricated a novel ultrathin Li metal anode via electrochemically depositing Li metal on a graphene nested carbon cloth, as shown in Figure 6C(a). Through the surface modification with graphene and ZnO seeds, a thickness-controllable and dendrite-free deposition was achieved. Ideally, the electrochemical deposition could precisely adjust the thickness of the Li deposit by controlling the conditions. However, the quality of deposited Li metal film, including the surface morphology, SEI composition, surface homogeneity, and film density, may challenge the application of this approach. Meanwhile, dendrites can form during the electrochemical deposition process.

Additionally, a thermal infusion strategy was proposed for a thin Li metal anode fabrication because of the low melting point of Li (190 °C). When using the thermal infusion method, the substrates must have high thermal stability, and the wettability of Li metal was highly determined by the surface properties of the substrates. Guo's group reported a facile thermal diffusion approach to preparing ultrathin Li metal anodes via coating various functional lithiophilic organic

materials on the surface of the substrate (Figure 6C (b)). The wettability of molten Li was tuned by combining new chemical bonds between molten Li and additives with -COOH, -OH, or  $-\text{NH}_2$  groups. As a result, an ultrathin Li metal anode with a thickness of  $10-40~\mu\text{m}$  was obtained, where the thickness of Li metal could be tuned by controlling the molten temperature and lithiophilic property of the substrate. Moreover, some inorganic materials, such as Ag, Si, Si, ZnO, And reduced graphene oxide (rGO), are also capable of improving the wettability of the substrate with molten Li. The inorganic coating layers were formed on the substrate by using electroplating, ALD, and chemical vapor deposition.

Furthermore, thin Li metal anodes also can be prepared via advanced thin-film fabrication technologies, such as PLD and VTVD. For example, a thin Li metal film of 1  $\mu$ m was fabricated on a Cu current collector by PLD technology, shown in Figure 6C(c). The thickness of the Li metal deposit can be adjusted by the processing time. The uniformity and density of the deposited Li film are also considerable. However, the biggest challenges may derive from the equipment's limitations. Currently, these technologies are utilized only at the lab scale with limited industrialization.

Different from the above designs for thin Li metal anode, the anode-free configuration is proposed to achieve higher energy density, which is feasible only for ASLBs using a Li-containing cathode. In this protocol, the Li resource in the cathode will be deposited onto the current collector to form an anode in the first cycle, which forms the most Li in the anode half-cell. Recently, Lee and Han et al. reported a highly effective Li-free anode fabricated by combining a thin Ag-C composite layer on a Cu current collector for high energy density ASLBs (Figure 6C (d)).<sup>27</sup> The Ag nanoparticles produce uniform Li metal deposition nucleation, and the carbon layer protects Li from reaction with sulfide SE. As a result, a 0.6 Ah punch cell exhibited CE of >99.8% and excellent capacity retention after more than 1000 cycles at 0.5C. For anode-free configurations, Li metal comes entirely from cathode materials, where there is no additional Li metal or other anode materials. Therefore, the anode-free design faces low CE (<99.5%) derived from the formation of SEI and extreme volume expansion of Li deposition.87 In addition, the anode-free design has also experience limited application in ASLBs using Li-free cathodes, such as S and FeS2, which are potential candidates for high energy density ASLBs.

In conclusion, the excess Li metal in ASLBs limits the cell-level energy density. The mechanical method (roll-to-roll), electrochemical deposition, thermal infusion strategy, and advanced thin-film fabrication technologies (such as PLD and VTVD) are promising to fabricate thin Li film with a minimal thickness. However, there are still challenges faced with these strategies for the quality of as-prepared Li, such as surface uniformity, bulk density, surface composition, new dendrites, and more. The anode-free configuration enables a significant increase in the energy density of ASLBs, but it still faces challenges, such as low CE and the limitation in using Li-free cathodes. Further investigation of these approaches is necessary to fabricate reliable thin Li metal anodes for ASLBs.

4. Architectural Design for High Energy Density Sulfide Electrolyte-Based ASLBs in Cell and Pack Level. Beyond the optimization of the cathode, electrolyte, and anode layers in ASLBs, the architectural design of ASLBs plays a significant role in delivering high energy, when it is extended to the cell

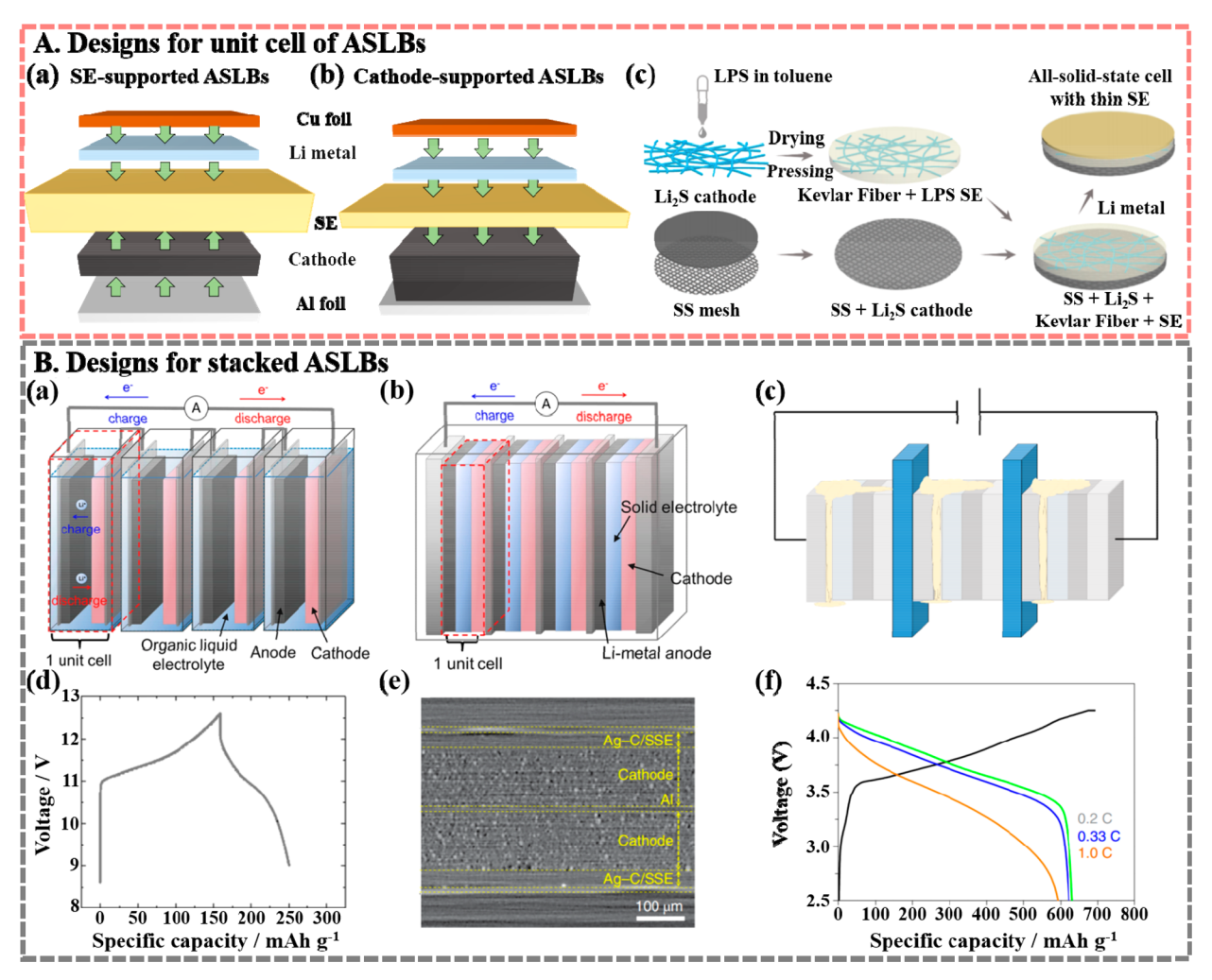


Figure 7. Architectural design of the high-energy ASLBs: (A) Unit cell. Schematic of (a) electrolyte-supported, (b) cathode-supported types, and (c) the fabrication process of a cathode-supported ASLBs. Reproduced with permission from ref 88. Copyright 2019 American Chemical Society.) (B) Stacked cells. Schematic of serial connected (a) LIBs using liquid electrolyte and (b) ASLBs. (Reproduced with permission from ref 90. Copyright 2015 Springer Nature.) (c) ASLB with triple cells in series connections and (d) corresponding galvanostatic charge—discharge profiles. (Reproduced with permission from ref 89. Copyright 2020 American Chemical Society.) (e) X-ray computed tomography of the ASLB with bicell structure and (f) corresponding galvanostatic charge—discharge profiles. (Reproduced with permission from ref 27. Copyright 2020 Springer Nature.)

level and stacking level. Because of the nonflowing nature of SEs, the architectural design of ASLBs differs from conventional liquid LIBs. In this section, the design of the unit cell and stacked cells will be briefly discussed.

As illustrated in Figure 7A, the conventional unit cell of ASLBs is a sheet-type structure. Considering the component that provides the mechanical strength for the ASLBs, the architecture structures of the unit cell can be roughly divided into the electrolyte-supported ASLBs (Figure 7A(a)) and cathode-supported ASLBs (Figure 7A(b)). Most reported ASLBs are the former type where the electrolyte is very thick to maintain a robust structure, and the cathode and Li are pressed on it. However, when the thickness is decreased to dozens of micrometers, such as the required 50  $\mu$ m, the electrolyte is too brittle to be handled. An effective method is to transfer the thin electrolyte onto a prepared thick cathode layer coated in a robust current collector and then stack with Li foil. The cathode-supported ASLBs not only deliver higher energy density but also show promising prospects for roll-toroll application in industry. Xu et al. reported a cathodesupported ASLB where the cathode mixture of Li<sub>2</sub>S-LiI,

PTFE, VGCF, and SEs were embedded into a stainless steel mesh and a thin Kevlar fiber reinforced SE is directly pressed onto the cathode layer (Figure 7A (c)). <sup>88</sup> The robust cathode layer provided high mechanical strength to the whole ASLB. In addition, the approach that the electrolyte layer is directly coated onto the cathode layer (such as the approach discussed in section 2.1 High-Voltage Cathode for High-Energy Density Sulfide Electrolyte-Based ASLBs) is also adopted to establish an intimate contact between cathode and electrolyte in cathode-supported ASLBs. <sup>51,54</sup>

The stackable feature of ASLBs enables batteries with high energy at the pack level. To achieve a high voltage output, the batteries are connected in series, whereas the batteries are connected in parallel to deliver high current. Compared with the necessary separation for each unit cell in series-connected conventional liquid LIBs (Figure 7B (a)), a bipolar stacking configuration in ASLBs is beneficial to reduce the number of current collectors and extra packing materials, where the unit cells are directly stacked together and connected in series (Figure 7B (b)). Homann et al. designed a triple cell battery package (Figure 7B (c)), in which a working voltage ranging

from 9 to 12.5 V was obtained (Figure 7B (d)). 89 Most recently, Lee et al. reported an ASLB with parallel-connected bicell structure, where cathode layers are coated on both sides of Al and an anode-free design is included (Figure 7B (e)). 27 Impressively, a 0.6 Ah pouch-type full cell was successfully obtained (Figure 7B (f)). According to the above discussion, area-oversized current collectors may be favorable to address the ionic short-cut caused by the flowing of polymer electrolyte. Additionally, compared with a Cu collector, the stainless steel collector may minimize corrosion caused by sulfide SEs.

**5.** Enhancing Energy Density of Other Solid Electrolytes. Each kind of SE exhibits its unique mechanical, chemical, physical, and electrochemical properties, and the strategies applied to enhance their energy density are various. The previous discussion is based on sulfide SEs, whereas other kinds of SEs have also demonstrated the potential for developing high-energy ASLBs. In this section, other typical SEs with high ion conductivity (>10<sup>-4</sup> S cm<sup>-1</sup>) are briefly discussed, including oxides, halides, and some composites.

5.1. Oxide Solid-State Electrolytes. As one of the promising SEs, metal oxide SEs exhibit a wide ESW, high air stability, and high mechanical stiffness but relatively low ion conductivity and poor interfacial contact. In order to improve the energy density in metal oxide ASLBs, strategies that reduce the SE thickness, increase the IC, and decrease its interface resistance are employed. In this section, various methods that enable enhancement of energy density and reduce the metal oxide interfacial resistance will be discussed in detail.

Similar to sulfide SEs, a direct and feasible approach to improve the energy density of ASLBs is to minimize the thickness of oxide SEs. The reduced thickness of SEs not only decreases the total mass of ASLBs but also decreases the length of ion conduction pathway. Compared to the metal sulfide, oxide electrolyte has higher chemical stability with organic solvents. Therefore, a thin oxide SE membrane can be fabricated by coating or casting methods. The thickness of the composite membranes can be tuned by controlling the doctor blade gap. Di and Guo et al. reported a method to fabricate flexible and ion-conducting SE membranes with a thickness of 40  $\mu$ m by coating an LLZO/PEO solution. 92 Additionally, various thin-film fabrication technologies, such as metal organic chemical vapor deposition, laser-assisted chemical vapor deposition, electro-spinning, and aerosol deposition, were also developed to prepare thin oxide SEs. 93,94

Moreover, the improvement of reversible capacity and corresponding energy density can be obtained by enhancing the bulk IC, which is determined by the crystal phase structure, grain size, and density of oxide SEs. Therefore, the enhancement of ion conductivity of oxide SEs can be obtained through element substitution to construct new crystal structures. The element substitutions, such as Al, Cr, Ta, and Nb, enable creating more Li vacancies and change the lattice size and shape, which promote Li ion conduction in oxide SEs. 95-97 For example, the NASICON-type LiTi<sub>2</sub>(PO<sub>4</sub>)<sub>3</sub> can obtain bulk conductivity of  $\sim 1.77 \times 10^{-3}$  S cm<sup>-1</sup> by doping Al and Cr elements. 96 The different ratios of doping elements resulted in a large difference of ion conductivity. The ion conductivity of  $\text{Li}_{1.4}\text{Al}_x\text{Cr}_{0.4-x}\text{Ti}_{1.6}(\text{PO}_4)_3$  (x = 0-0.4) tended to increase with the amount of Al increasing. The  $\text{Li}_{1.4}\text{Al}_{x}\text{Cr}_{0.4-x}\text{Ti}_{1.6}(\text{PO}_{4})_{3}$ obtained a maximum total conductivity of  $1.27 \times 10^{-3} \text{ S cm}^$ at x = 0.3 at 25 °C. In addition, the synthesis process, such as sintering temperature, additives, and sintering approaches, also

results in different grain boundary and densification of bulk ceramics, which highly impact the ion conductivity. 94

On the other hand, the high rigidity of oxide SEs negatively affects interfacial contact and inhibits ion conduction at the interface. On the Li metal side, similar to some sulfide SEs, the Ti<sup>4+</sup>- and Ge<sup>4+</sup>-containing oxide SEs, including perovskite-type, NASICON-type, and LISICON-type electrolytes, exhibit poor chemical stability against Li metal because of the reduction of Ti<sup>4+</sup> and Ge<sup>4+,95,96,98</sup> The interphase formed by oxide SEs decomposition resulted in significant increases in interfacial resistance, more than 1 order of magnitude greater than the original state.<sup>99</sup> To improve the interface contact, in the cathode half-cell side, a tiny amount of liquid electrolyte or polymer gel electrolyte is employed as an interlayer to minimize interfacial resistance. On the Li metal side, the thin artificial interfacial layers with high chemical stability and ion conductivity are introduced between oxide SEs and Li metal. For example, to improve interfacial contact, the ultrathin Al<sub>2</sub>O<sub>3</sub> and Si interfacial layers were introduced between oxide SEs (LATP and LLZO) and Li metal by ALD and plasmaenhanced chemical vapor deposition (PECVD), respectively. The Al<sub>2</sub>O<sub>3</sub> coating layer can be converted to a Li-Al-O ionconducting layer through a reaction with Li metal, promoting ion conduction at the interface. <sup>101</sup> The interfacial contact was significantly improved because of the introduction of a superlithiophilic amorphous Si layer, leading to interfacial resistance dramatically dropping between Li metal and LLZO SEs from 925 to 127  $\Omega$  cm<sup>2.102</sup> In addition, John B. Goodenough's group reported that LiN3 was used as interlayer to improve interfacial compatibility between garnet-type oxide SEs and Li metal. Compared to Al<sub>2</sub>O<sub>3</sub> and Si, LiN<sub>3</sub> possesses the advantages of high ion conductivity (around 10<sup>-3</sup> S cm<sup>-1</sup> at RT) and excellent chemical stability against Li metal. 103 As a result, the full cell coupled with LiFePO<sub>4</sub> cathode exhibited a CE of almost 100% and a long-term cycling life over 300 charge-discharge cycles at 40 °C. Moreover, organic (polymer) materials are also explored as interfacial layers in oxide ASLBs. For example, a cross-linked Li<sup>+</sup> polymer conductor was reported to construct a stable interphase between LATP and Li metal. 104 The elastic polymer layer not only provided great interfacial compatibility and a physical barrier between LATP and Li metal but also facilitated ion conduction at the interface. When pairing with LiFePO<sub>4</sub> cathode, the full cell delivered superlong cycling stability and ultrahigh CE of 99.8%-100%.

In conclusion, oxide SEs have the characteristic of high chemical stability and mechanical strength but low ion conductivity. Their excellent chemical stability offers flexible methods to construct a thin SE membrane in ASLBs, which is favorable for improving battery energy density. The bulky ion conductivity of oxide SEs can be further enhanced via element substitution. However, the high mechanical strength and low conductivity lead to serious interfacial resistance between oxide SEs and electrode materials. To overcome the interfacial incompatibility, different organic or inorganic artificial interlayers are developed in ASLBs. Compared to organic (polymer) interlayer, the lithiophilic inorganic interphase shows a more promising prospect for high energy density ASLBs owing to its high ion conductivity and interfacial compatibility.

5.2. Halide Solid-State Electrolytes. Halide SEs, such as Li<sub>3</sub>InCl<sub>6</sub>, Li<sub>3</sub>YCl<sub>6</sub>, Li<sub>3</sub>YBr<sub>6</sub>, Li<sub>3</sub>ErCl<sub>6</sub>, Li<sub>3-x</sub>M<sub>1-x</sub>Zr<sub>x</sub>Cl<sub>6</sub> (M = Er, Y), Li<sub>x</sub>ScCl<sub>3+x</sub> (x = 2.5, 3, 3.5, and 4), and so forth, exhibit high

IC (>10<sup>-4</sup> S cm<sup>-1</sup> at RT), which sheds light on a new type of promising electrolyte for ASLBs beyond sulfide SEs. 105 The study of halide SEs dates back to the 1930s but has not been brought to the forefront because most of them, like Li halides LiX (X = F, Cl, Br, and I), fluorite-structured halides, and spinel-structured halides, showed relatively low IC ( $\leq 10^{-5}$  S cm<sup>-1</sup>) and instability at RT. In 2018, Asano et al. reported two rare-earth-based halide SEs, Li<sub>3</sub>YCl<sub>6</sub> and Li<sub>3</sub>YBr<sub>6</sub>, which delivered ionic conductivity of over  $1 \times 10^{-3} \text{ S cm}^{-1}$  at RT and maintained excellent stability. 107 Very recently, Li et al. reported that Li<sub>3</sub>InCl<sub>6</sub> synthesized through mechanochemical and water-mediated methods delivered high ICs of  $1.49 \times 10^{-3}$ and  $2.04 \times 10^{-3}$  S cm<sup>-1</sup>, respectively. Notably, these halide SEs are not novel materials, but the ionic conductivities have improved with better understanding and optimized synthesis. Therefore, the discussion surrounding high-energy ASLBs related to halide SEs is based on these representative candidates because of their high IC and phase stability at RT.

Halide-based ASLBs are expected to deliver ultrahigh energy density for material chemistry because of their high IC as well as good compatibility with electrodes. Compared with sulfide SEs, halides, especially fluorides and chlorides, often possess higher oxidation stability due to higher oxidation potentials of  $F^-$  (>6 V) and  $Cl^-$  (>4 V) compared to  $S^{2-}$  (<2.6 V). 110,111 The recently reported Li<sub>3</sub>ScCl<sub>6</sub> exhibited an ultrahigh IC of 3  $\times$  10<sup>-3</sup> S cm<sup>-1</sup> at RT and a wide ESW of 0.9–4.3 V. 112 The high upper limit for the stability window of halides liberates the conventional high-voltage CAM from the protective layer, which is inevitable in sulfide-based ASLBs. 113 Furthermore, some chloride compounds exhibit better deformability than oxides, which is helpful to construct intimate contact and reduce the interface resistance. 114 However, on the Li metal anode side, halide SEs show poor stability because the metallic cations in halide SEs are easily reduced by Li metal. Therefore, interface engineering is necessary to stabilize the interphase between halide SEs and Li metal. Similar to sulfide SEs, Li halides LiX (X = F, Cl, and I) often utilize artificial interface layers because of their high stability with Li metal.

Various synthesis strategies, like dry and wet methods, also enlighten the development of halide-based ASLBs with celllevel high energy density. Generally, the design ideas for halide SEs are similar to that of the aforementioned methods of sulfide SEs, i.e., developing a thin SE layer, high mass loading cathode, and stabilized Li metal anode with reduced thickness. Thanks to their natural malleability, it is easy to get a dense SE layer and cathode layer through a simple cold pressing method without further sintering. The binder-assisted dry method applied for sulfide SEs can be easily replicated. It should be noted that treatment temperature is crucial in this method, because the phase transition of some halides varies with temperature and may accompany a decrease in IC. In addition, the solution-based strategies are also feasible for halide SEs. Different from sulfide SEs, some halide SEs, like Li<sub>3</sub>InCl<sub>6</sub> and Li<sub>3</sub>Y<sub>x</sub>In<sub>1-x</sub>Cl<sub>6</sub>, exhibit high stability with humidity. More specifically, Li<sub>3</sub>InCl<sub>6</sub> was highlighted with having good processability in water. 108,109,115 Even though the humidity leads to a negative effect on the IC of the Li<sub>2</sub>InCl<sub>6</sub> because of some side reactions, the IC can be recovered via heat treatment at a relatively low temperature (260 °C). In addition, Li<sub>3</sub>InCl<sub>6</sub> synthesized in a water-mediated system could obtain high ion conductivity after a dehydration process at 200 °C. The feature of water stability provides more

possibilities for low-cost fabrication processing, alternative binders, and environmental feasibility.

5.3. Composite Polymer Electrolyte. Composite polymer electrolytes (CPEs) combine the merits of multiple components to deliver unique performance superior to each individual contributor. 116 Most CPEs are based on solid polymer electrolytes (SPEs), which have the characteristics of thin thickness, flexibility, processability, and excellent interfacial compatibility. Various techniques, such as solution casting, tape casting, spin coating, hot pressing, screen printing, and melting intercalation are feasible for the SE film preparation in large-scale CPE-based ASLBs. 117 Intimate interface contact with both cathode and anode is obtained in CPEs, especially for the in situ polymerization approach. This method is highlighted for fabricating an integrated interface and enhanced interfacial compatibility between CPEs and electrodes. 118 However, SPEs are usually criticized for their poor IC at RT. For example, the PEO system was well-studied as a solid-state electrolyte in ASLBs, but the IC was on the order of only 10<sup>-6</sup> S cm<sup>-1</sup> at RT. 119 Moreover, the dendrite issue and high-voltage stability inhibited the application of SPE-based ASLBs because of the soft property and instable electrochemical stability. Therefore, to address these challenges, inorganic fillers, i.e., CPEs, are mixed with SPEs.

Recent research has reported that CPEs could deliver higher IC than single-phase SPEs at RT, which leads to outstanding performance on the level of  $10^{-4}$  S cm<sup>-1</sup> being achieved when introducing ion conductors in polymers. The properties of CPE, such as IC, morphology, distribution, and ratio, are strongly determined by inorganic fillers. Generally, the ion conduction in single-phase SPE is attributed to ion hopping in the amorphous polymer chains. Therefore, it was widely accepted that the introduction of inorganic fillers which decrease the crystallinity of the polymer would accelerate ion transport. More importantly, the introduction of ion conductors generates more ion transport pathways. When the content of fillers is low, the situation usually is defined as "ceramic in polymer (CIP)"; the ion conduction is mainly mediated by polymers and the surface of the fillers, because there is no percolation of these fillers. 125,126 Liu et al. developed a CPE by incorporating polyacryloitrile-LiClO<sub>4</sub> with 15 wt % electrospun  $Li_{0.33}La_{0.557}TiO_3$  nanowires to obtain an outstanding IC of  $2.4\times10^{-4}~S~cm^{-1}$ . Compared with the particle morphology, 1D nanowires generated a longrange Li<sup>+</sup> transfer channel along the surface of the nanofibers, which contribute almost 2 orders of magnitude greater IC. When the fillers account for the main fraction in the CPEs, i.e., the situation named "polymer in ceramic (PIC)", the percolation fabricated by fillers also contributes to ion conduction. However, most PICs show IC lower than that of CIP because the high fraction of inorganic fillers leads to porosity increase and the formation of filler agglomerates, which impedes ion conductive pathways along with the interface. 125 Moreover, the alignment of fillers greatly affects the ion conductivity. Liu et al. compared the effect of Li<sup>+</sup>conductive nanowires being either randomly distributed or well-aligned in CPEs. 124 Impressively, 1 order of magnitude higher improvement in IC was achieved in the CPE with wellaligned fillers, which is ascribed to the reduced crossing junctions on the surfaces of aligned nanowires. Architectural design that combines a cathode-supported unit cell and bilayer stacking greatly boosts the cell-level energy density.

Architectural design that combines a cathode-supported unit cell and bilayer stacking greatly boosts the cell-level energy density.

The stabilities of CPEs when coupled with high-voltage cathode and Li metal anode are also critical. First, the ESW of CPEs is desired to be greater than 4.3 V (vs Li<sup>+</sup>/Li) to match the high-voltage cathode. Compared with the single-phase SPE, the incorporation with inorganic fillers is proven that lead to a higher voltage limit. For example, PEO-based SPE has a low ESW (<4 V) because of the reactive terminal -OH group, while Chen et al. reported that the ESW of CPE compositing PEO with Li<sub>6.4</sub>La<sub>3</sub>Zr<sub>1.4</sub>Ta<sub>0.4</sub>O<sub>12</sub> is stable up to 5.0 V. <sup>125</sup> Second, a stable interface between CSEs and CAM is necessary. Qiu et al. reported that delithiated LiCoO2 is a strong oxidizer, which accelerates the degradation of PEO and loss of CAM. To avoid this interface reaction, a coating layer of Li<sub>1.4</sub>Al<sub>0.4</sub>Ti<sub>1.6</sub>(PO<sub>4</sub>)<sub>3</sub> on LCO was employed. Moreover, the stability with Li metal is crucial to CPEs. Generally, all polymers have reactions with Li metal anode to generate an SEI layer, whose property greatly affects the performance. High IC and chemical stability with Li metal are desired for SEI to deliver a low-impedance interface. On the other hand, the dendrite issue still hinders SPEs. Impressively, CPEs are usually able to suppress dendrites because of their enhanced mechanical strength and ion transference.7

In summary, CPEs are highlighted for manufacturing feasibility of high-energy ASLBs, because they are more promising than most other ASLBs. However, the relatively lower IC at RT is still the main obstacle, even though a conductivity of 10<sup>-4</sup> S cm<sup>-1</sup> has been achieved. To enable the ASLBs working at RT, the IC should be further enhanced, which needs further investigation on the mechanism of ion conduction in CPEs and corresponding electrolyte design. Additionally, like the ESW and stability with both cathode and Li metal anode, the low IC can be addressed by controlling the inorganic fillers and modifying the polymers.

6. Summary and Perspective. In summary, to achieve celllevel high-energy ASLBs, especially using sulfide SEs, the recent progress and remaining challenges have been reviewed. Although numerous works have reported improved energy density relative to the active materials, the energy density of cell-level ASLBs is low, which is largely due to the high thickness of the electrolyte layer, low mass loading of the cathode, and excessive Li metal. Research contributions regarding materials and electrochemistry in ASLBs are essential for their development and have been discussed in previous reviews. In this Review, we specifically summarize the challenges and strategies in manufacturing of cell-level highenergy sulfide electrolyte-based ASLBs. First, based on the unique properties of sulfide SEs, processing methods like slurry coating, drying processing, and templating are introduced for fabricating a thin SE layer. The development of high-voltage and high-capacity cathodes is then discussed separately. For high-voltage cathodes, the effects of particle size distribution, carbon additives, and binders are specifically discussed. For high-capacity cathodes, the promising solutions for improving the ion and electron accessibilities, ionic and electronic conductivities, and alleviating the volume expansion are reviewed. As for the Li metal anode, some effective strategies

for stabilizing the sulfide SEllLi interface and fabricating thin Li metal and even anode-free designs are introduced. In addition, the architectural design of the unit cell, like SE-supported and cathode-supported ASLBs, are compared. When extended to stacked cells, the discussion on parallel connected multi-cell structures and bipolar stacking series connections are included. In the end, the progress of other electrolytes, like oxides, halides, and SPE, in developing cell-level high energy ASLBs is briefly reviewed.

Although impressive progress has been made, there are still significant challenges faced for processing cell-level high-energy ASLBs using sulfide SEs. We summarized the corresponding challenges that need to be tackled in each section. Herein, we focus on only the energy density improvement in cell and stack levels for practical application of ASLBs: (1) The performance evaluation should also be conducted in a large-sized cell, like a pouch cell. Most reported ASLBs are operated in a pressurized cell with area of  $\sim 1$  cm<sup>-2</sup>, which exhibit considerable performance. However, like the performance degradation in LIBs from coin cell to pouch cells, the behavior of ASLBs in large-sized cells is also challenging. The mechanical strength of each layer is critical in the fabrication of ASLBs in a pouch cell. (2) Bipolar ASLBs exhibit high potential in large-scale energy storage, but the application of bipolar ASLBs in sulfide SE is scarce to date. The layer-by-layer stacking process challenges the mechanical strength of each layer. In addition to the electronic short circuit, it is important to avoid the short circuit caused by the internal ionic connection between unit cells. Meanwhile, the corrosion that occurs on the current collector under oxidation or reduction limits the use of conventional Cu or Al foil. Developing lightweight, anticorrosion, and highly conductive current collectors is critical for bipolar sulfide electrolyte-based ASLBs. (3) Large-scale processing techniques, like roll-to-roll manufacturing and solution casting, should be further investigated, which is significant for the transfer of ASLBs from lab to industrialization. One of the most challenging issues is the mechanical strength of the electrolyte layer when reducing the thickness to the required value. The selection of compatible binders and solvent is critical to obtaining a robust electrolyte layer for large-scale manufacturing accompanied by greatly sacrificed ionic conductivity. Meanwhile, it is important to further reduce the cost of ceramic electrolytes for industrial applications. (4) The processing environment of sulfide SEs is vital. It is essential to improve the air stability of sulfide SEs. If it is manufactured in an inert atmosphere, then it is important to control the environment strictly to reduce the side reactions and avoid the generation of toxic H<sub>2</sub>S gas. A deeper understanding of the material chemistry, manufacturing methods, and cell configuration will accelerate the development of ASLBs to meet the goal of high energy density for commercialization.

## AUTHOR INFORMATION

### **Corresponding Author**

Hongli Zhu — Department of Mechanical and Industrial Engineering, Northeastern University, Boston, Massachusetts 02115, United States; ⊚ orcid.org/0000-0003-1733-4333; Email: h.zhu@northeastern.edu

#### **Authors**

- Daxian Cao Department of Mechanical and Industrial Engineering, Northeastern University, Boston, Massachusetts 02115, United States
- Yuyue Zhao Department of Mechanical and Industrial Engineering, Northeastern University, Boston, Massachusetts 02115, United States
- Xiao Sun Department of Mechanical and Industrial Engineering, Northeastern University, Boston, Massachusetts 02115, United States
- Avi Natan Department of Mechanical and Industrial Engineering, Northeastern University, Boston, Massachusetts 02115. United States
- Ying Wang Department of Mechanical and Industrial Engineering, Northeastern University, Boston, Massachusetts 02115, United States
- Pengyang Xiang Department of Mechanical and Industrial Engineering, Northeastern University, Boston, Massachusetts 02115, United States
- Wei Wang Rogers Corporation Innovation Center, Burlington, Massachusetts 01803, United States

Complete contact information is available at: https://pubs.acs.org/10.1021/acsenergylett.0c01905

#### **Author Contributions**

D.C. and Y.Z. contributed equally to this work.

#### Notes

The authors declare no competing financial interest.

### **Biographies**

Daxian Cao is currently a postdoc in Mechanical and Industrial Engineering at Northeastern University. His research interests include advanced all-solid-state batteries and Li metal anode. He received his B.S. degree (2014) in Material Science and Engineering and Ph.D. degree (2019) in Electrical Engineering from Xi'an Jiaotong University.

Yuyue Zhao is currently a postdoctoral researcher at Northeastern University. His research focuses on flow batteries and solid-state-batteries. He received his Ph.D. degree from Dalian Institute of Chemical Physics (DICP) Chinese Academy of Sciences in 2018. He worked in Argonne National Laboratory as a postdoctoral fellow from 2018 to 2020.

Xiao Sun is currently a Ph.D. student at the Department of Mechanical and Industrial Engineering at Northeastern University. She received her M.S. in mechanical engineering department from Northeastern in 2019. Her research focuses on investigating materials for high-performance energy storage and developing all-solid-state batteries.

**Avi Natan** is a senior undergraduate student in the Department of Chemical Engineering at Northeastern University. He is interested in bioderived multifunctional materials and energy storage.

Ying Wang is a Ph.D. student in Professor Hongli Zhu's group at Northeastern University. She received her M.S. degree (2020) in the Department of Mechanical and Industrial Engineering from Northeastern University. She is interested in advanced manufacturing and multifunctional materials for energy storage.

Pengyang Xiang is a master's student at the Department of Mechanical and Industrial Engineering, Northeastern University. He received his B.S.E. degree (2019) in Electrical Engineering from the University of Iowa. His research interests include clean energy and sustainable materials.

Wei Wang is currently working as the Principal Innovator at Rogers Corporation focuses on developing and manufacturing high-performance materials and components for battery cells and packs. He received his Ph.D. in Materials Science and Engineering and M.S. in Electrical Engineering at the University of California, Riverside. His areas of expertise include functional materials synthesis and processing and battery cell and system development.

Hongli Zhu is currently an assistant professor at Northeastern University. From 2012 to 2015, she worked in the University of Maryland as a postdoc on energy storage and paper electronics. From 2009 to 2011, she conducted research on materials science and processing of biodegradable and renewable biomaterials from natural wood in the KTH Royal Institute of Technology in Sweden. https://coe.northeastern.edu/Research/hongli group/index.html

#### ACKNOWLEDGMENTS

H.Z. acknowledges financial support from the National Science Foundation Electrochemical Systems Program at Division of Chemical, Bioengineering, Environmental and Transport Systems (Award Number: CBET-1924534) and Rogers Corporation, United States.

#### REFERENCES

- (1) Placke, T.; Kloepsch, R.; Dühnen, S.; Winter, M. Lithium ion, lithium metal, and alternative rechargeable battery technologies: the odyssey for high energy density. *J. Solid State Electrochem.* **2017**, *21* (7), 1939–1964.
- (2) Cano, Z. P.; Banham, D.; Ye, S.; Hintennach, A.; Lu, J.; Fowler, M.; Chen, Z. Batteries and fuel cells for emerging electric vehicle markets. *Nature Energy* **2018**, 3 (4), 279–289.
- (3) Srinivasan, V. In *Batteries for vehicular applications*; AIP Conference Proceedings, American Institute of Physics, 2008; pp 283–296.
- (4) USABC Goals for Advanced High-Performance Batteries for Electric Vehicle (EV) Applications.
- (5) Zhang, Q.; Cao, D.; Ma, Y.; Natan, A.; Aurora, P.; Zhu, H. Sulfide-Based Solid-State Electrolytes: Synthesis, Stability, and Potential for All-Solid-State Batteries. *Adv. Mater.* **2019**, *31* (44), 1901131.
- (6) Weiss, M.; Simon, F. J.; Busche, M. R.; Nakamura, T.; Schröder, D.; Richter, F. H.; Janek, J. From Liquid- to Solid-State Batteries: Ion Transfer Kinetics of Heteroionic Interfaces. *Electrochemical Energy Reviews* **2020**, 3 (2), 221–238.
- (7) Cao, D.; Sun, X.; Li, Q.; Natan, A.; Xiang, P.; Zhu, H. Lithium Dendrite in All-Solid-State Batteries: Growth Mechanisms, Suppression Strategies, and Characterizations. *Matter* **2020**, *3* (5), 57.
- (8) Cao, D.; Zhang, Q.; Hafez, A. M.; Jiao, Y.; Ma, Y.; Li, H.; Cheng, Z.; Niu, C.; Zhu, H. Lignin-Derived Holey, Layered, and Thermally Conductive 3D Scaffold for Lithium Dendrite Suppression. *Small Methods* **2019**, *3* (5), 1800539.
- (9) Monroe, C.; Newman, J. The Impact of Elastic Deformation on Deposition Kinetics at Lithium/Polymer Interfaces. *J. Electrochem. Soc.* **2005**, *152* (2), A396–A404.
- (10) Yang, X.; Luo, J.; Sun, X. Towards high-performance solid-state Li–S batteries: from fundamental understanding to engineering design. *Chem. Soc. Rev.* **2020**, 49 (7), 2140–2195.
- (11) Umeshbabu, E.; Zheng, B.; Yang, Y. Recent Progress in All-Solid-State Lithium—Sulfur Batteries Using High Li-Ion Conductive Solid Electrolytes. *Electrochemical Energy Reviews* **2019**, 2 (2), 199–230.
- (12) Bruce, P. G.; Freunberger, S. A.; Hardwick, L. J.; Tarascon, J.-M. Li-O2 and Li-S batteries with high energy storage. *Nat. Mater.* **2012**, *11* (1), 19–29.
- (13) Cao, D.; Zhang, Y.; Nolan, A. M.; Sun, X.; Liu, C.; Sheng, J.; Mo, Y.; Wang, Y.; Zhu, H. Stable Thiophosphate-Based All-Solid-

- State Lithium Batteries through Conformally Interfacial Nanocoating. *Nano Lett.* **2020**, *20* (3), 1483–1490.
- (14) Zhao, W.; Yi, J.; He, P.; Zhou, H. Solid-State Electrolytes for Lithium-Ion Batteries: Fundamentals, Challenges and Perspectives. *Electrochemical Energy Reviews* **2019**, 2 (4), 574–605.
- (15) Ohno, S.; Banik, A.; Dewald, G. F.; Kraft, M. A.; Krauskopf, T.; Minafra, N.; Till, P.; Weiss, M.; Zeier, W. G. Materials design of ionic conductors for solid state batteries. *Progress in Energy* **2020**, 2 (2), 022001.
- (16) Zhu, Y.; He, X.; Mo, Y. First principles study on electrochemical and chemical stability of solid electrolyte—electrode interfaces in all-solid-state Li-ion batteries. *J. Mater. Chem. A* **2016**, 4 (9), 3253–3266.
- (17) Han, F.; Westover, A. S.; Yue, J.; Fan, X.; Wang, F.; Chi, M.; Leonard, D. N.; Dudney, N. J.; Wang, H.; Wang, C. High electronic conductivity as the origin of lithium dendrite formation within solid electrolytes. *Nature Energy* **2019**, *4* (3), 187–196.
- (18) Whiteley, J. M.; Taynton, P.; Zhang, W.; Lee, S.-H. Ultra-thin Solid-State Li-Ion Electrolyte Membrane Facilitated by a Self-Healing Polymer Matrix. *Adv. Mater.* **2015**, *27* (43), 6922–6927.
- (19) Zhang, Z.; Chen, S.; Yang, J.; Wang, J.; Yao, L.; Yao, X.; Cui, P.; Xu, X. Interface re-engineering of Li10GeP2S12 electrolyte and lithium anode for all-solid-state lithium batteries with ultralong cycle life. ACS Appl. Mater. Interfaces 2018, 10 (3), 2556–2565.
- (20) Woo, J. H.; Trevey, J. E.; Cavanagh, A. S.; Choi, Y. S.; Kim, S. C.; George, S. M.; Oh, K. H.; Lee, S.-H. Nanoscale Interface Modification of LiCoO2by Al2O3Atomic Layer Deposition for Solid-State Li Batteries. *J. Electrochem. Soc.* **2012**, *159* (7), A1120–A1124.
- (21) Xie, D.; Chen, S.; Zhang, Z.; Ren, J.; Yao, L.; Wu, L.; Yao, X.; Xu, X. High ion conductive Sb2O5-doped  $\beta$ -Li3PS4 with excellent stability against Li for all-solid-state lithium batteries. *J. Power Sources* **2018**, 389, 140–147.
- (22) Ulissi, U.; Agostini, M.; Ito, S.; Aihara, Y.; Hassoun, J. All solid-state battery using layered oxide cathode, lithium-carbon composite anode and thio-LISICON electrolyte. *Solid State Ionics* **2016**, *296*, 13–17
- (23) Yamada, T.; Ito, S.; Omoda, R.; Watanabe, T.; Aihara, Y.; Agostini, M.; Ulissi, U.; Hassoun, J.; Scrosati, B. All solid-state lithium—sulfur battery using a glass-type P2S5—Li2S electrolyte: benefits on anode kinetics. *J. Electrochem. Soc.* **2015**, *162* (4), A646.
- (24) Yao, X.; Liu, D.; Wang, C.; Long, P.; Peng, G.; Hu, Y.-S.; Li, H.; Chen, L.; Xu, X. High-energy all-solid-state lithium batteries with ultralong cycle life. *Nano Lett.* **2016**, *16* (11), 7148–7154.
- (25) Zhang, Q.; Peng, G.; Mwizerwa, J. P.; Wan, H.; Cai, L.; Xu, X.; Yao, X. Nickel sulfide anchored carbon nanotubes for all-solid-state lithium batteries with enhanced rate capability and cycling stability. *J. Mater. Chem. A* **2018**, 6 (25), 12098–12105.
- (26) Ulissi, U.; Ito, S.; Hosseini, S. M.; Varzi, A.; Aihara, Y.; Passerini, S. High Capacity All-Solid-State Lithium Batteries Enabled by Pyrite-Sulfur Composites. *Adv. Energy Mater.* **2018**, 8 (26), 1801462.
- (27) Lee, Y.-G.; Fujiki, S.; Jung, C.; Suzuki, N.; Yashiro, N.; Omoda, R.; Ko, D.-S.; Shiratsuchi, T.; Sugimoto, T.; Ryu, S.; Ku, J. H.; Watanabe, T.; Park, Y.; Aihara, Y.; Im, D.; Han, I. T. High-energy long-cycling all-solid-state lithium metal batteries enabled by silver—carbon composite anodes. *Nature Energy* **2020**, *5* (4), 299–308.
- (28) Hatzell, K. B.; Chen, X. C.; Cobb, C. L.; Dasgupta, N. P.; Dixit, M. B.; Marbella, L. E.; McDowell, M. T.; Mukherjee, P. P.; Verma, A.; Viswanathan, V.; Westover, A. S.; Zeier, W. G. Challenges in Lithium Metal Anodes for Solid-State Batteries. *ACS Energy Letters* **2020**, *5* (3), 922–934.
- (29) Randau, S.; Weber, D. A.; Kötz, O.; Koerver, R.; Braun, P.; Weber, A.; Ivers-Tiffée, E.; Adermann, T.; Kulisch, J.; Zeier, W. G.; Richter, F. H.; Janek, J. Benchmarking the performance of all-solid-state lithium batteries. *Nature Energy* **2020**, *5* (3), 259–270.
- (30) Miura, A.; Rosero-Navarro, N. C.; Sakuda, A.; Tadanaga, K.; Phuc, N. H. H.; Matsuda, A.; Machida, N.; Hayashi, A.; Tatsumisago, M. Liquid-phase syntheses of sulfide electrolytes for all-solid-state lithium battery. *Nature Reviews Chemistry* **2019**, 3 (3), 189–198.

- (31) Zhang, Q.; Cao, D.; Ma, Y.; Natan, A.; Aurora, P.; Zhu, H. Sulfide-Based Solid-State Electrolytes: Synthesis, Stability, and Potential for All-Solid-State Batteries. *Adv. Mater.* **2019**, *31*, 1901131.
- (32) Inada, T.; Takada, K.; Kajiyama, A.; Kouguchi, M.; Sasaki, H.; Kondo, S.; Watanabe, M.; Murayama, M.; Kanno, R. Fabrications and properties of composite solid-state electrolytes. *Solid State Ionics* **2003**, 158 (3), 275–280.
- (33) Nam, Y. J.; Oh, D. Y.; Jung, S. H.; Jung, Y. S. Toward practical all-solid-state lithium-ion batteries with high energy density and safety: Comparative study for electrodes fabricated by dry- and slurry-mixing processes. *J. Power Sources* **2018**, *375*, 93–101.
- (34) Li, M.; Frerichs, J. E.; Kolek, M.; Sun, W.; Zhou, D.; Huang, C. J.; Hwang, B. J.; Hansen, M. R.; Winter, M.; Bieker, P. Solid-State Lithium—Sulfur Battery Enabled by Thio-LiSICON/Polymer Composite Electrolyte and Sulfurized Polyacrylonitrile Cathode. *Adv. Funct. Mater.* **2020**, 30 (14), 1910123.
- (35) Yersak, T.; Salvador, J. R.; Schmidt, R. D.; Cai, M. Hot Pressed, Fiber-Reinforced (Li2S)70(P2SS)30 Solid-State Electrolyte Separators for Li Metal Batteries. ACS Applied Energy Materials 2019, 2 (5), 3523–3531.
- (36) Li, Y.; Cao, D.; Arnold, W.; Ren, Y.; Liu, C.; Jasinski, J. B.; Druffel, T.; Cao, Y.; Zhu, H.; Wang, H. Regulated lithium ionic flux through well-aligned channels for lithium dendrite inhibition in solid-state batteries. *Energy Storage Materials* **2020**, *31*, 344–351.
- (37) Kim, D. H.; Lee, Y.-H.; Song, Y. B.; Kwak, H.; Lee, S.-Y.; Jung, Y. S. Thin and Flexible Solid Electrolyte Membranes with Ultrahigh Thermal Stability Derived from Solution-Processable Li Argyrodites for All-Solid-State Li-Ion Batteries. ACS Energy Letters 2020, 5 (3), 718–727.
- (38) Nam, Y. J.; Cho, S.-J.; Oh, D. Y.; Lim, J.-M.; Kim, S. Y.; Song, J. H.; Lee, Y.-G.; Lee, S.-Y.; Jung, Y. S. Bendable and Thin Sulfide Solid Electrolyte Film: A New Electrolyte Opportunity for Free-Standing and Stackable High-Energy All-Solid-State Lithium-Ion Batteries. *Nano Lett.* **2015**, *15* (5), 3317–3323.
- (39) Kato, Y.; Shiotani, S.; Morita, K.; Suzuki, K.; Hirayama, M.; Kanno, R. All-Solid-State Batteries with Thick Electrode Configurations. *J. Phys. Chem. Lett.* **2018**, *9* (3), 607–613.
- (40) Nie, K.; Hong, Y.; Qiu, J.; Li, Q.; Yu, X.; Li, H.; Chen, L., Interfaces Between Cathode and Electrolyte in Solid State Lithium Batteries: Challenges and Perspectives. *Front. Chem.* **2018**, *6* (616). DOI: 10.3389/fchem.2018.00616
- (41) Manthiram, A. A reflection on lithium-ion battery cathode chemistry. *Nat. Commun.* **2020**, *11* (1), 1550.
- (42) Wang, X.; Ding, Y.-L.; Deng, Y.-P.; Chen, Z. Ni-Rich/Co-Poor Layered Cathode for Automotive Li-Ion Batteries: Promises and Challenges. *Adv. Energy Mater.* **2020**, *10* (12), 1903864.
- (43) Shi, T.; Tu, Q.; Tian, Y.; Xiao, Y.; Miara, L. J.; Kononova, O.; Ceder, G. High Active Material Loading in All-Solid-State Battery Electrode via Particle Size Optimization. *Adv. Energy Mater.* **2020**, *10* (1), 1902881.
- (44) Wang, C.; Liang, J.; Hwang, S.; Li, X.; Zhao, Y.; Adair, K.; Zhao, C.; Li, X.; Deng, S.; Lin, X.; Yang, X.; Li, R.; Huang, H.; Zhang, L.; Lu, S.; Su, D.; Sun, X. Unveiling the critical role of interfacial ionic conductivity in all-solid-state lithium batteries. *Nano Energy* **2020**, *72*, 104686.
- (45) Nakamura, T.; Amezawa, K.; Kulisch, J.; Zeier, W. G.; Janek, J. Guidelines for All-Solid-State Battery Design and Electrode Buffer Layers Based on Chemical Potential Profile Calculation. *ACS Appl. Mater. Interfaces* **2019**, *11* (22), 19968–19976.
- (46) Wang, C.; Li, X.; Zhao, Y.; Banis, M. N.; Liang, J.; Li, X.; Sun, Y.; Adair, K. R.; Sun, Q.; Liu, Y.; Zhao, F.; Deng, S.; Lin, X.; Li, R.; Hu, Y.; Sham, T.-K.; Huang, H.; Zhang, L.; Yang, R.; Lu, S.; Sun, X. Manipulating Interfacial Nanostructure to Achieve High-Performance All-Solid-State Lithium-Ion Batteries. *Small Methods* **2019**, 3 (10), 1900261.
- (47) Strauss, F.; Bartsch, T.; de Biasi, L.; Kim, A. Y.; Janek, J.; Hartmann, P.; Brezesinski, T. Impact of Cathode Material Particle Size on the Capacity of Bulk-Type All-Solid-State Batteries. *ACS Energy Letters* **2018**, 3 (4), 992–996.

- (48) Wang, C.; Yu, R.; Hwang, S.; Liang, J.; Li, X.; Zhao, C.; Sun, Y.; Wang, J.; Holmes, N.; Li, R.; Huang, H.; Zhao, S.; Zhang, L.; Lu, S.; Su, D.; Sun, X. Single crystal cathodes enabling high-performance all-solid-state lithium-ion batteries. *Energy Storage Materials* **2020**, *30*, 98–103
- (49) Zhang, W.; Leichtweiß, T.; Culver, S. P.; Koerver, R.; Das, D.; Weber, D. A.; Zeier, W. G.; Janek, J. The Detrimental Effects of Carbon Additives in Li10GeP2S12-Based Solid-State Batteries. ACS Appl. Mater. Interfaces 2017, 9 (41), 35888–35896.
- (50) Noh, S.; Nichols, W. T.; Cho, M.; Shin, D. Importance of mixing protocol for enhanced performance of composite cathodes in all-solid-state batteries using sulfide solid electrolyte. *J. Electroceram.* **2018**, 40 (4), 293–299.
- (51) Ates, T.; Keller, M.; Kulisch, J.; Adermann, T.; Passerini, S. Development of an all-solid-state lithium battery by slurry-coating procedures using a sulfidic electrolyte. *Energy Storage Materials* **2019**, *17*, 204–210.
- (52) Deng, S.; Sun, Y.; Li, X.; Ren, Z.; Liang, J.; Doyle-Davis, K.; Liang, J.; Li, W.; Norouzi Banis, M.; Sun, Q.; Li, R.; Hu, Y.; Huang, H.; Zhang, L.; Lu, S.; Luo, J.; Sun, X. Eliminating the Detrimental Effects of Conductive Agents in Sulfide-Based Solid-State Batteries. ACS Energy Letters 2020, 5 (4), 1243–1251.
- (53) Hippauf, F.; Schumm, B.; Doerfler, S.; Althues, H.; Fujiki, S.; Shiratsuchi, T.; Tsujimura, T.; Aihara, Y.; Kaskel, S. Overcoming binder limitations of sheet-type solid-state cathodes using a solvent-free dry-film approach. *Energy Storage Materials* **2019**, *21*, 390–398.
- (54) Oh, D. Y.; Nam, Y. J.; Park, K. H.; Jung, S. H.; Kim, K. T.; Ha, A. R.; Jung, Y. S. Slurry-Fabricable Li+-Conductive Polymeric Binders for Practical All-Solid-State Lithium-Ion Batteries Enabled by Solvate Ionic Liquids. *Adv. Energy Mater.* **2019**, *9* (16), 1802927.
- (55) Yamamoto, M.; Terauchi, Y.; Sakuda, A.; Takahashi, M. Binderfree sheet-type all-solid-state batteries with enhanced rate capabilities and high energy densities. *Sci. Rep.* **2018**, *8* (1), 1212.
- (56) Yang, X.; Li, X.; Adair, K.; Zhang, H.; Sun, X. Structural Design of Lithium—Sulfur Batteries: From Fundamental Research to Practical Application. *Electrochemical Energy Reviews* **2018**, *1* (3), 239–293.
- (57) Yu, C.; Ganapathy, S.; de Klerk, N. J. J.; Roslon, I.; van Eck, E. R. H.; Kentgens, A. P. M.; Wagemaker, M. Unravelling Li-Ion Transport from Picoseconds to Seconds: Bulk versus Interfaces in an Argyrodite Li6PSSCl–Li2S All-Solid-State Li-Ion Battery. J. Am. Chem. Soc. 2016, 138 (35), 11192–11201.
- (58) Choi, H. U.; Jin, J. S.; Park, J.-Y.; Lim, H.-T. Performance improvement of all-solid-state Li-S batteries with optimizing morphology and structure of sulfur composite electrode. *J. Alloys Compd.* **2017**, 723, 787–794.
- (59) Nagao, M.; Hayashi, A.; Tatsumisago, M. Sulfur—carbon composite electrode for all-solid-state Li/S battery with Li2S—P2S5 solid electrolyte. *Electrochim. Acta* **2011**, *56* (17), 6055–6059.
- (60) Han, Q.; Li, X.; Shi, X.; Zhang, H.; Song, D.; Ding, F.; Zhang, L. Outstanding cycle stability and rate capabilities of the all-solid-state Li–S battery with a Li7P3S11 glass-ceramic electrolyte and a coreshell S@BP2000 nanocomposite. *J. Mater. Chem. A* **2019**, 7 (8), 3895–3902.
- (61) Suzuki, K.; Mashimo, N.; Ikeda, Y.; Yokoi, T.; Hirayama, M.; Kanno, R. High Cycle Capability of All-Solid-State Lithium—Sulfur Batteries Using Composite Electrodes by Liquid-Phase and Mechanical Mixing. ACS Applied Energy Materials 2018, 1 (6), 2373—2377.
- (62) Yan, H.; Wang, H.; Wang, D.; Li, X.; Gong, Z.; Yang, Y. In Situ Generated Li2S—C Nanocomposite for High-Capacity and Long-Life All-Solid-State Lithium Sulfur Batteries with Ultrahigh Areal Mass Loading. *Nano Lett.* **2019**, *19* (5), 3280–3287.
- (63) Han, F.; Yue, J.; Fan, X.; Gao, T.; Luo, C.; Ma, Z.; Suo, L.; Wang, C. High-Performance All-Solid-State Lithium—Sulfur Battery Enabled by a Mixed-Conductive Li2S Nanocomposite. *Nano Lett.* **2016**, *16* (7), 4521–4527.
- (64) Lin, Z.; Liu, Z.; Dudney, N. J.; Liang, C. Lithium Superionic Sulfide Cathode for All-Solid Lithium—Sulfur Batteries. *ACS Nano* **2013**, 7 (3), 2829—2833.

- (65) Li, X.; Liang, J.; Luo, J.; Wang, C.; Li, X.; Sun, Q.; Li, R.; Zhang, L.; Yang, R.; Lu, S.; Huang, H.; Sun, X. High-Performance Li—SeSx All-Solid-State Lithium Batteries. *Adv. Mater.* **2019**, *31* (17), 1808100
- (66) Zhang, Y.; Sun, Y.; Peng, L.; Yang, J.; Jia, H.; Zhang, Z.; Shan, B.; Xie, J. Se as eutectic accelerator in sulfurized polyacrylonitrile for high performance all-solid-state lithium-sulfur battery. *Energy Storage Materials* **2019**, 21, 287–296.
- (67) Koerver, R.; Zhang, W.; de Biasi, L.; Schweidler, S.; Kondrakov, A. O.; Kolling, S.; Brezesinski, T.; Hartmann, P.; Zeier, W. G.; Janek, J. Chemo-mechanical expansion of lithium electrode materials on the route to mechanically optimized all-solid-state batteries. *Energy Environ. Sci.* **2018**, *11* (8), 2142—2158.
- (68) Doux, J.-M.; Yang, Y.; Tan, D. H. S.; Nguyen, H.; Wu, E. A.; Wang, X.; Banerjee, A.; Meng, Y. S. Pressure effects on sulfide electrolytes for all solid-state batteries. *J. Mater. Chem. A* **2020**, 8 (10), 5049–5055
- (69) Yao, X.; Huang, N.; Han, F.; Zhang, Q.; Wan, H.; Mwizerwa, J. P.; Wang, C.; Xu, X. High-Performance All-Solid-State Lithium—Sulfur Batteries Enabled by Amorphous Sulfur-Coated Reduced Graphene Oxide Cathodes. *Adv. Energy Mater.* **2017**, 7 (17), 1602923.
- (70) Zhu, Y.; He, X.; Mo, Y. Origin of Outstanding Stability in the Lithium Solid Electrolyte Materials: Insights from Thermodynamic Analyses Based on First-Principles Calculations. *ACS Appl. Mater. Interfaces* **2015**, 7 (42), 23685–23693.
- (71) Cheng, X.-B.; Yan, C.; Chen, X.; Guan, C.; Huang, J.-Q.; Peng, H.-J.; Zhang, R.; Yang, S.-T.; Zhang, Q. Implantable Solid Electrolyte Interphase in Lithium-Metal Batteries. *Chem.* **2017**, 2 (2), 258–270.
- (72) Han, F.; Yue, J.; Zhu, X.; Wang, C. Suppressing Li Dendrite Formation in Li2S-P2SS Solid Electrolyte by LiI Incorporation. *Adv. Energy Mater.* **2018**, 8 (18), 1703644.
- (73) Zhao, F.; Sun, Q.; Yu, C.; Zhang, S.; Adair, K.; Wang, S.; Liu, Y.; Zhao, Y.; Liang, J.; Wang, C.; Li, X.; Li, X.; Xia, W.; Li, R.; Huang, H.; Zhang, L.; Zhao, S.; Lu, S.; Sun, X. Ultrastable Anode Interface Achieved by Fluorinating Electrolytes for All-Solid-State Li Metal Batteries. ACS Energy Letters 2020, 5 (4), 1035–1043.
- (74) Xu, R.; Han, F.; Ji, X.; Fan, X.; Tu, J.; Wang, C. Interface engineering of sulfide electrolytes for all-solid-state lithium batteries. *Nano Energy* **2018**, *53*, 958–966.
- (75) Liang, J.; Li, X.; Zhao, Y.; Goncharova, L. V.; Wang, G.; Adair, K. R.; Wang, C.; Li, R.; Zhu, Y.; Qian, Y.; Zhang, L.; Yang, R.; Lu, S.; Sun, X. In Situ Li3 PS4 Solid-State Electrolyte Protection Layers for Superior Long-Life and High-Rate Lithium-Metal Anodes. *Adv. Mater.* **2018**, *30* (45), 1804684.
- (76) Sang, L.; Bassett, K. L.; Castro, F. C.; Young, M. J.; Chen, L.; Haasch, R. T.; Elam, J. W.; Dravid, V. P.; Nuzzo, R. G.; Gewirth, A. A. Understanding the Effect of Interlayers at the Thiophosphate Solid Electrolyte/Lithium Interface for All-Solid-State Li Batteries. *Chem. Mater.* **2018**, 30 (24), 8747–8756.
- (77) Wang, C.; Adair, K. R.; Liang, J.; Li, X.; Sun, Y.; Li, X.; Wang, J.; Sun, Q.; Zhao, F.; Lin, X.; Li, R.; Huang, H.; Zhang, L.; Yang, R.; Lu, S.; Sun, X. Solid-State Plastic Crystal Electrolytes: Effective Protection Interlayers for Sulfide-Based All-Solid-State Lithium Metal Batteries. *Adv. Funct. Mater.* **2019**, 29 (26), 1900392.
- (78) Bouchard, P.; Guerin, P.-E.; St-Amant, G.; Laroche, G. Process for laminating a thin film of lihium by controlled detachment. US 5,528,920, 1996.
- (79) Schnell, J.; Günther, T.; Knoche, T.; Vieider, C.; Köhler, L.; Just, A.; Keller, M.; Passerini, S.; Reinhart, G. All-solid-state lithiumion and lithium metal batteries paving the way to large-scale production. *J. Power Sources* **2018**, 382, 160–175.
- (80) Deng, W.; Zhu, W.; Zhou, X.; Liu, Z. Graphene nested porous carbon current collector for lithium metal anode with ultrahigh areal capacity. *Energy Storage Materials* **2018**, *15*, 266–273.
- (81) Wang, S. H.; Yue, J.; Dong, W.; Zuo, T. T.; Li, J. Y.; Liu, X.; Zhang, X. D.; Liu, L.; Shi, J. L.; Yin, Y. X.; Guo, Y. G. Tuning wettability of molten lithium via a chemical strategy for lithium metal anodes. *Nat. Commun.* **2019**, *10* (1), 4930.

- (82) Zhang, R.; Chen, X.; Shen, X.; Zhang, X.-Q.; Chen, X.-R.; Cheng, X.-B.; Yan, C.; Zhao, C.-Z.; Zhang, Q. Coralloid Carbon Fiber-Based Composite Lithium Anode for Robust Lithium Metal Batteries. *Joule* **2018**, 2 (4), 764–777.
- (83) Liang, Z.; Lin, D.; Zhao, J.; Lu, Z.; Liu, Y.; Liu, C.; Lu, Y.; Wang, H.; Yan, K.; Tao, X.; Cui, Y. Composite lithium metal anode by melt infusion of lithium into a 3D conducting scaffold with lithiophilic coating. *Proc. Natl. Acad. Sci. U. S. A.* **2016**, *113* (11), 2862–7.
- (84) Wang, C.; Gong, Y.; Liu, B.; Fu, K.; Yao, Y.; Hitz, E.; Li, Y.; Dai, J.; Xu, S.; Luo, W.; Wachsman, E. D.; Hu, L. Conformal, Nanoscale ZnO Surface Modification of Garnet-Based Solid-State Electrolyte for Lithium Metal Anodes. *Nano Lett.* **2017**, *17* (1), 565–571
- (85) Lin, D.; Liu, Y.; Liang, Z.; Lee, H. W.; Sun, J.; Wang, H.; Yan, K.; Xie, J.; Cui, Y. Layered reduced graphene oxide with nanoscale interlayer gaps as a stable host for lithium metal anodes. *Nat. Nanotechnol.* **2016**, *11* (7), 626–32.
- (86) Ogawa, M.; Kanda, R.; Yoshida, K.; Uemura, T.; Harada, K. High-capacity thin film lithium batteries with sulfide solid electrolytes. *J. Power Sources* **2012**, 205, 487–490.
- (87) Chen, J.; Li, Q.; Pollard, T. P.; Fan, X.; Borodin, O.; Wang, C. Electrolyte design for Li metal-free Li batteries. *Mater. Today* **2020**, DOI: 10.1016/j.mattod.2020.04.004.
- (88) Xu, R.; Yue, J.; Liu, S.; Tu, J.; Han, F.; Liu, P.; Wang, C. Cathode-Supported All-Solid-State Lithium—Sulfur Batteries with High Cell-Level Energy Density. ACS Energy Letters 2019, 4 (5), 1073—1079.
- (89) Homann, G.; Meister, P.; Stolz, L.; Brinkmann, J. P.; Kulisch, J.; Adermann, T.; Winter, M.; Kasnatscheew, J. High-Voltage All-Solid-State Lithium Battery with Sulfide-Based Electrolyte: Challenges for the Construction of a Bipolar Multicell Stack and How to Overcome Them. ACS Applied Energy Materials 2020, 3 (4), 3162–3168.
- (90) Gambe, Y.; Sun, Y.; Honma, I. Development of Bipolar Allsolid-state Lithium Battery Based on Quasi-solid-state Electrolyte Containing Tetraglyme-LiTFSA Equimolar Complex. Sci. Rep. 2015, 5 (1), 8869.
- (91) Manthiram, A.; Yu, X.; Wang, S. Lithium battery chemistries enabled by solid-state electrolytes. *Nature Reviews Materials* **2017**, 2 (4), 16103.
- (92) Zhang, J.; Zhao, N.; Zhang, M.; Li, Y.; Chu, P. K.; Guo, X.; Di, Z.; Wang, X.; Li, H. Flexible and ion-conducting membrane electrolytes for solid-state lithium batteries: Dispersion of garnet nanoparticles in insulating polyethylene oxide. *Nano Energy* **2016**, 28, 447–454.
- (93) Inada, R.; Ishida, K.-i.; Tojo, M.; Okada, T.; Tojo, T.; Sakurai, Y. Properties of aerosol deposited NASICON-type Li1.5Al0.5Ge1.5-(PO4)3 solid electrolyte thin films. *Ceram. Int.* **2015**, *41* (9), 11136–11142.
- (94) Liu, Q.; Geng, Z.; Han, C.; Fu, Y.; Li, S.; He, Y.-b.; Kang, F.; Li, B. Challenges and perspectives of garnet solid electrolytes for all solid-state lithium batteries. *J. Power Sources* **2018**, *389*, 120–134.
- (95) El-Shinawi, H.; Regoutz, A.; Payne, D. J.; Cussen, E. J.; Corr, S. A. NASICON LiM2(PO4)3 electrolyte (M = Zr) and electrode (M = Ti) materials for all solid-state Li-ion batteries with high total conductivity and low interfacial resistance. *J. Mater. Chem. A* **2018**, 6 (13), 5296–5303.
- (96) Zhang, P.; Wang, H.; Si, Q.; Matsui, M.; Takeda, Y.; Yamamoto, O.; Imanishi, N. High lithium ion conductivity solid electrolyte of chromium and aluminum co-doped NASICON-type LiTi2(PO4)3. *Solid State Ionics* **2015**, 272, 101–106.
- (97) Mukhopadhyay, S.; Thompson, T.; Sakamoto, J.; Huq, A.; Wolfenstine, J.; Allen, J. L.; Bernstein, N.; Stewart, D. A.; Johannes, M. D. Structure and Stoichiometry in Supervalent Doped Li7La3Zr2O12. *Chem. Mater.* **2015**, 27 (10), 3658–3665.
- (98) Sun, C.; Liu, J.; Gong, Y.; Wilkinson, D. P.; Zhang, J. Recent advances in all-solid-state rechargeable lithium batteries. *Nano Energy* **2017**, *33*, 363–386.

- (99) Hartmann, P.; Leichtweiss, T.; Busche, M. R.; Schneider, M.; Reich, M.; Sann, J.; Adelhelm, P.; Janek, J. Degradation of NASICON-Type Materials in Contact with Lithium Metal: Formation of Mixed Conducting Interphases (MCI) on Solid Electrolytes. *J. Phys. Chem. C* 2013, 117 (41), 21064–21074.
- (100) Jiang, Z.; Xie, H.; Wang, S.; Song, X.; Yao, X.; Wang, H. Perovskite Membranes with Vertically Aligned Microchannels for All-Solid-State Lithium Batteries. *Adv. Energy Mater.* **2018**, 8 (27), 1801433.
- (101) Liu, Y.; Sun, Q.; Zhao, Y.; Wang, B.; Kaghazchi, P.; Adair, K. R.; Li, R.; Zhang, C.; Liu, J.; Kuo, L. Y.; Hu, Y.; Sham, T. K.; Zhang, L.; Yang, R.; Lu, S.; Song, X.; Sun, X. Stabilizing the Interface of NASICON Solid Electrolyte against Li Metal with Atomic Layer Deposition. ACS Appl. Mater. Interfaces 2018, 10 (37), 31240–31248. (102) Luo, W.; Gong, Y.; Zhu, Y.; Fu, K. K.; Dai, J.; Lacey, S. D.; Wang, C.; Liu, B.; Han, X.; Mo, Y.; Wachsman, E. D.; Hu, L. Transition from Superlithiophobicity to Superlithiophilicity of Garnet Solid-State Electrolyte. J. Am. Chem. Soc. 2016, 138 (37), 12258–62. (103) Xu, H.; Li, Y.; Zhou, A.; Wu, N.; Xin, S.; Li, Z.; Goodenough, J. B. Li3N-Modified Garnet Electrolyte for All-Solid-State Lithium Metal Batteries Operated at 40 degrees C. Nano Lett. 2018, 18 (11), 7414–7418.
- (104) Zhou, W.; Wang, S.; Li, Y.; Xin, S.; Manthiram, A.; Goodenough, J. B. Plating a Dendrite-Free Lithium Anode with a Polymer/Ceramic/Polymer Sandwich Electrolyte. *J. Am. Chem. Soc.* **2016**, *138* (30), 9385–8.
- (105) Li, X.; Liang, J.; Yang, X.; Adair, K. R.; Wang, C.; Zhao, F.; Sun, X. Progress and perspectives on halide lithium conductors for all-solid-state lithium batteries. *Energy Environ. Sci.* **2020**, *13* (5), 1429–1461.
- (106) Bachman, J. C.; Muy, S.; Grimaud, A.; Chang, H.-H.; Pour, N.; Lux, S. F.; Paschos, O.; Maglia, F.; Lupart, S.; Lamp, P.; Giordano, L.; Shao-Horn, Y. Inorganic Solid-State Electrolytes for Lithium Batteries: Mechanisms and Properties Governing Ion Conduction. *Chem. Rev.* **2016**, *116* (1), 140–162.
- (107) Asano, T.; Sakai, A.; Ouchi, S.; Sakaida, M.; Miyazaki, A.; Hasegawa, S. Solid Halide Electrolytes with High Lithium-Ion Conductivity for Application in 4 V Class Bulk-Type All-Solid-State Batteries. *Adv. Mater.* **2018**, *30* (44), 1803075.
- (108) Li, X.; Liang, J.; Luo, J.; Norouzi Banis, M.; Wang, C.; Li, W.; Deng, S.; Yu, C.; Zhao, F.; Hu, Y.; Sham, T.-K.; Zhang, L.; Zhao, S.; Lu, S.; Huang, H.; Li, R.; Adair, K. R.; Sun, X. Air-stable Li3InCl6 electrolyte with high voltage compatibility for all-solid-state batteries. *Energy Environ. Sci.* **2019**, *12* (9), 2665–2671.
- (109) Li, X.; Liang, J.; Chen, N.; Luo, J.; Adair, K. R.; Wang, C.; Banis, M. N.; Sham, T.-K.; Zhang, L.; Zhao, S.; Lu, S.; Huang, H.; Li, R.; Sun, X. Water-Mediated Synthesis of a Superionic Halide Solid Electrolyte. *Angew. Chem., Int. Ed.* **2019**, 58 (46), 16427–16432.
- (110) Richards, W. D.; Miara, L. J.; Wang, Y.; Kim, J. C.; Ceder, G. Interface Stability in Solid-State Batteries. *Chem. Mater.* **2016**, 28 (1), 266–273
- (111) Wang, S.; Bai, Q.; Nolan, A. M.; Liu, Y.; Gong, S.; Sun, Q.; Mo, Y. Lithium Chlorides and Bromides as Promising Solid-State Chemistries for Fast Ion Conductors with Good Electrochemical Stability. *Angew. Chem., Int. Ed.* **2019**, *58* (24), 8039–8043.
- (112) Liang, J.; Li, X.; Wang, S.; Adair, K. R.; Li, W.; Zhao, Y.; Wang, C.; Hu, Y.; Zhang, L.; Zhao, S.; Lu, S.; Huang, H.; Li, R.; Mo, Y.; Sun, X. Site-Occupation-Tuned Superionic LixScCl3+xHalide Solid Electrolytes for All-Solid-State Batteries. *J. Am. Chem. Soc.* **2020**, 142 (15), 7012–7022.
- (113) Wang, C.; Liang, J.; Jiang, M.; Li, X.; Mukherjee, S.; Adair, K.; Zheng, M.; Zhao, Y.; Zhao, F.; Zhang, S.; Li, R.; Huang, H.; Zhao, S.; Zhang, L.; Lu, S.; Singh, C. V.; Sun, X. Interface-assisted in-situ growth of halide electrolytes eliminating interfacial challenges of all-inorganic solid-state batteries. *Nano Energy* **2020**, *76*, 105015.
- (114) Park, K.-H.; Kaup, K.; Assoud, A.; Zhang, Q.; Wu, X.; Nazar, L. F. High-Voltage Superionic Halide Solid Electrolytes for All-Solid-State Li-Ion Batteries. *ACS Energy Letters* **2020**, *5* (2), 533–539.

- (115) Li, X.; Liang, J.; Adair, K. R.; Li, J.; Li, W.; Zhao, F.; Hu, Y.; Sham, T.-K.; Zhang, L.; Zhao, S.; Lu, S.; Huang, H.; Li, R.; Chen, N.; Sun, X. Origin of Superionic Li3Y1–xInxCl6 Halide Solid Electrolytes with High Humidity Tolerance. *Nano Lett.* **2020**, 20 (6), 4384–4392.
- (116) Zou, Z.; Li, Y.; Lu, Z.; Wang, D.; Cui, Y.; Guo, B.; Li, Y.; Liang, X.; Feng, J.; Li, H.; Nan, C.-W.; Armand, M.; Chen, L.; Xu, K.; Shi, S. Mobile Ions in Composite Solids. *Chem. Rev.* **2020**, *120* (9), 4169–4221.
- (117) Arya, A.; Sharma, A. L. Polymer electrolytes for lithium ion batteries: a critical study. *Ionics* **2017**, 23 (3), 497–540.
- (118) Liu, T.; Zhang, J.; Han, W.; Zhang, J.; Ding, G.; Dong, S.; Cui, G. In Situ Polymerization for Integration and Interfacial Protection Towards Solid State Lithium Batteries. *J. Electrochem. Soc.* **2020**, *167* (7), 070527.
- (119) Wright, P. V. Electrical conductivity in ionic complexes of poly(ethylene oxide). *Br. Polym. J.* **1975**, *7* (5), 319–327.
- (120) Liu, W.; Liu, N.; Sun, J.; Hsu, P.-C.; Li, Y.; Lee, H.-W.; Cui, Y. Ionic Conductivity Enhancement of Polymer Electrolytes with Ceramic Nanowire Fillers. *Nano Lett.* **2015**, *15* (4), 2740–2745.
- (121) Fu, K.; Gong, Y.; Dai, J.; Gong, A.; Han, X.; Yao, Y.; Wang, C.; Wang, Y.; Chen, Y.; Yan, C.; Li, Y.; Wachsman, E. D.; Hu, L. Flexible, solid-state, ion-conducting membrane with 3D garnet nanofiber networks for lithium batteries. *Proc. Natl. Acad. Sci. U. S. A.* **2016**, *113* (26), 7094–7099.
- (122) Lin, D.; Liu, W.; Liu, Y.; Lee, H. R.; Hsu, P.-C.; Liu, K.; Cui, Y. High Ionic Conductivity of Composite Solid Polymer Electrolyte via In Situ Synthesis of Monodispersed SiO2 Nanospheres in Poly(ethylene oxide). *Nano Lett.* **2016**, *16* (1), 459–465.
- (123) Chen, R.-J.; Zhang, Y.-B.; Liu, T.; Xu, B.-Q.; Lin, Y.-H.; Nan, C.-W.; Shen, Y. Addressing the Interface Issues in All-Solid-State Bulk-Type Lithium Ion Battery via an All-Composite Approach. *ACS Appl. Mater. Interfaces* **2017**, *9* (11), 9654–9661.
- (124) Liu, W.; Lee, S. W.; Lin, D.; Shi, F.; Wang, S.; Sendek, A. D.; Cui, Y. Enhancing ionic conductivity in composite polymer electrolytes with well-aligned ceramic nanowires. *Nature Energy* **2017**, *2* (5), 17035.
- (125) Chen, L.; Li, Y.; Li, S.-P.; Fan, L.-Z.; Nan, C.-W.; Goodenough, J. B. PEO/garnet composite electrolytes for solid-state lithium batteries: From "ceramic-in-polymer" to "polymer-inceramic. *Nano Energy* **2018**, *46*, 176–184.
- (126) Huo, H.; Chen, Y.; Luo, J.; Yang, X.; Guo, X.; Sun, X. Rational Design of Hierarchical "Ceramic-in-Polymer" and "Polymer-in-Ceramic" Electrolytes for Dendrite-Free Solid-State Batteries. *Adv. Energy Mater.* **2019**, *9* (17), 1804004.
- (127) Bag, S.; Zhou, C.; Kim, P. J.; Pol, V. G.; Thangadurai, V. LiF modified stable flexible PVDF-garnet hybrid electrolyte for high performance all-solid-state Li–S batteries. *Energy Storage Materials* **2020**, 24, 198–207.
- (128) Zhu, P.; Yan, C.; Dirican, M.; Zhu, J.; Zang, J.; Selvan, R. K.; Chung, C.-C.; Jia, H.; Li, Y.; Kiyak, Y.; Wu, N.; Zhang, X. Li0.33La0.557TiO3 ceramic nanofiber-enhanced polyethylene oxide-based composite polymer electrolytes for all-solid-state lithium batteries. *J. Mater. Chem. A* **2018**, *6* (10), 4279–4285.
- (129) Zhang, B.; Chen, L.; Hu, J.; Liu, Y.; Liu, Y.; Feng, Q.; Zhu, G.; Fan, L.-Z. Solid-state lithium metal batteries enabled with high loading composite cathode materials and ceramic-based composite electrolytes. *J. Power Sources* **2019**, 442, 227230.
- (130) Shi, X.; Ma, N.; Wu, Y.; Lu, Y.; Xiao, Q.; Li, Z.; Lei, G. Fabrication and electrochemical properties of LATP/PVDF composite electrolytes for rechargeable lithium-ion battery. *Solid State Ionics* **2018**, 325, 112–119.
- (131) Qiu, J.; Liu, X.; Chen, R.; Li, Q.; Wang, Y.; Chen, P.; Gan, L.; Lee, S.-J.; Nordlund, D.; Liu, Y.; Yu, X.; Bai, X.; Li, H.; Chen, L. Enabling Stable Cycling of 4.2 V High-Voltage All-Solid-State Batteries with PEO-Based Solid Electrolyte. *Adv. Funct. Mater.* 2020, 30 (22), 1909392.